Eur. J. Mineral.
2006, **18**, 673–689

Order and anti-order in olivine I: Structural response to temperature

ROLF HEINEMANN[1], HERBERT KROLL[1], ARMIN KIRFEL[2] and BRUNO BARBIER[2]

[1]Institut für Mineralogie, Westfälische Wilhelms-Universität, Corrensstr. 24, 48149 Münster, Germany
*Corresponding author, e-mail: kroll@nwz.uni-muenster.de
[2]Mineralogisch-Petrologisches Institut, Poppelsdorfer Schloss, 53115 Bonn, Germany

Abstract: The crystal structure of $Fe_{0.48}Mg_{0.52}[SiO_4]$ olivine from the Boseti volcano, Ethiopia, has been investigated by single-crystal X-ray diffractometry at temperatures between 20 °C and 900 °C. For temperatures up to 600 °C, data were collected on crystals equilibrated at 600 °C. These data can therefore be assumed to reflect structural changes that are exclusively caused by thermal effects, whereas data collected between 600 °C and 900 °C carry additional information about the Fe^{2+},Mg equilibrium distribution. The *in situ* experiments at elevated temperatures were complemented by ambient temperature data collections on quenched crystals in order to check for possible Fe^{2+} and Mg redistributions during quenching. Such effects were found absent in crystals quenched from 800 °C or below.

The derived temperature dependence of the Fe^{2+},Mg site distribution is

$$\ln K_D = 0.4422(\pm 0.0070) - 140.0(\pm 6.5)/T\,(K)$$

according to which Fe^{2+} progressively anti-orders into the M1 "octahedral" site as temperature is raised. A reverse ordering reaction at ≈650 °C leading to a strong segregation of Fe^{2+} into the other "octahedral" site, M2, as reported by Redfern *et al*. (2000), could not be detected.

Both the <M1-O> and <M2-O> mean bond distances continuously increase with temperature, exhibiting, however, a change in the increase rate at about 600 °C which conforms with an enrichment of the larger Fe^{2+} cation on the M1 site and its concomitant depletion on M2. In terms of bond lengths, the octahedral distortion of the M2 site is larger than that of M1. The opposite is true for the distortion defined in terms of the angles subtended at the cation site. Similar to the <M-O> distances, the behaviour of the distortion parameters both of which increase above 600 °C reflects the Fe^{2+},Mg anti-order. The relative magnitudes as well as the variation with temperature of both bond length and angular distortions can be rationalized considering the different geometrical environments of the M1 and M2 sites. With respect to isotropic displacement parameters, $U(M1)_{equiv}$ is found larger than $U(M2)_{equiv}$ at all temperatures, also at variance with Redfern *et al*. (2000).

Key-words: olivine, order, anti-order, distortion, thermal expansion, solid solution, geospeedometry.

Introduction

Increasing cation order at increasing temperatures is a phenomenon rarely observed in minerals. Usually, increasing temperatures result in increasing disorder. Familiar examples of this behaviour include rock-forming minerals like feldspars where at high temperatures Al and Si disorder over the tetrahedral sites or orthopyroxenes where Fe^{2+} and Mg disorder over the octahedral sites. Olivine, $(Fe^{2+},Mg)^{M2}(Mg,Fe^{2+})^{M1}[SiO_4]$, however, behaves differently.

The endmembers of the olivine series are forsterite, $Mg_2[SiO_4]$ (Fo), and fayalite, $Fe_2[SiO_4]$ (Fa). Fe^{2+} and Mg fractionate over two non-equivalent "octahedral" sites, M1 and M2. The order-disorder process is termed non-convergent because M1 and M2 do not converge to symmetry equivalence even when Fe^{2+} and Mg become randomly distributed. Consequently, the state of full disorder is not associated with a phase transition (Thompson, 1969, 1970).

In natural Mg-rich olivines (≈Fa10) from metamorphic rocks, Fe^{2+} is found somewhat enriched in the M2 site, whereas in olivines from volcanic rocks Fe^{2+} shows some preference for M1 (Aikawa *et al.*, 1985; Princivalle, 1990; Freiheit *et al.*, 2000). This suggests that at high temperatures Fe^{2+} favours M1 whereas upon slow cooling it progressively fractionates into M2 and thus a state of full disorder is passed at some temperature. Smyth & Hazen (1973) as well as Heinemann *et al.* (1999) observed that in samples heated to 900 °C, the Fe^{2+} concentration in M1 increased with rising temperature. Recently, Artioli *et al.* (1995) and Rinaldi *et al.* (2000) performed *in situ* single-crystal neutron diffraction studies on natural olivines (Fa10 and Fa12) at tempera-

0935-1221/06/0018-0673 $ 7.65
DOI: 10.1127/0935-1221/2006/0018-0673

Table 1. Electron microprobe analysis.

oxides	observed	sigma[a]	atoms	observed	sigma[a]	adjusted
SiO_2	34.85	0.37	Si	0.9947	0.0068	1.0000
MgO	23.97	0.21	Mg	1.0197	0.0083	1.0165
FeO	39.37	0.40	Fe	0.9398	0.0110	0.9351
MnO	1.67	0.09	Mn	0.0405	0.0022	0.0402
CaO	0.27	0.03	Ca	0.0082	0.0009	0.0082
sum M				2.0082		2.0000
sum total	100.14			3.0029		3.0000
Σval				7.9952		8.0000
Δ(M-T)[b]				0.0376		0.0000
X_{Fa}[c]						0.4791
X_{Fo}[c]						0.5209

[a] sigma: estimated standard deviation
[b] Δ(M-T): difference between charge excess in the M sites and charge deficiency in the T sites
[c] X_{Fa}= Fe / (Fe+Mg), X_{Fo}= 1 – X_{Fa}

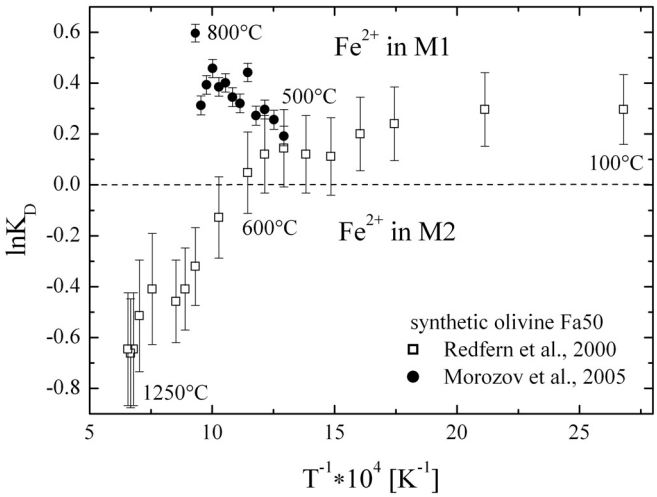

Fig. 1. Variation of $\ln K_D$ with inverse temperature of olivine Fa50. Open squares: Results of Redfern *et al*. (2000) obtained from *in situ* neutron powder diffraction. Filled circles: Results of Morozov *et al*. (2001, 2005) obtained from Mößbauer spectra of quenched powder samples. The distribution coefficient K_D is defined as $K_D = X_{Fe}^{M1} X_{Mg}^{M2} / X_{Fe}^{M2} X_{Mg}^{M1}$. Site occupancies are symbolized by $X_{element}^{site}$.

tures up to 1300 °C. They also found Fe^{2+} initially enriched in M1. Then, however, the cation ordering sharply reversed at 850 °C above which temperature Fe^{2+} clearly preferred to fractionate into M2. The state of full disorder was passed at 900 °C. A similar behaviour was found by Redfern *et al.* (2000) for synthetic polycrystalline olivine (Fa50). In their case, the state of full disorder was reached at a temperature as low as 650 °C.

The order-disorder behaviour reported by Redfern *et al.* (2000) is obviously in contrast not only to the results of Heinemann *et al.* (2003) obtained by single-crystal X-ray diffraction on quenched and *in situ* heated natural olivine Fa48 but also to the results of Mößbauer studies performed by Morozov *et al.* (2001, 2005) on quenched synthetic olivine Fa50 (see Fig. 1).

The present study augments the earlier work of Heinemann *et al.* (2003) with the aim to investigate the olivine structure as a function of temperature, including its thermal expansion, the distortion of the M1 and M2 octahedra, the behaviour of the atomic displacement parameters, and the variation of the Fe^{2+},Mg distribution. To this purpose and since it has been repeatedly demonstrated that the correlation between the cation thermal displacement parameters and the site occupancies (Kroll *et al.*, 1997; Heinemann *et al*., 1999, 2000) is one of the principal obstacles in deriving reliable cation distributions from X-ray and/or neutron scattering experiments special efforts have been made to control this effect.

Experimental

Sampling and electron microprobe analysis

Two olivine phenocrysts have been handpicked from a small chip of a trachytic rock collected by Brotzu *et al.* (1980, sample Bo421) from the Boseti volcano, Main Ethiopian Rift, Ethiopia. The phenocrysts were cut into pieces which were subjected to microscopic investigation and X-ray diffraction. Four pieces (numbered Bo-2, 5, 8, 10) were free of inclusions, showed distinct extinctions under the microscope and produced sharp diffraction spots on Laue photographs. Several of the remaining pieces were selected for chemical composition analyses by electron microprobing with a CAMECA SX-100 (operated by J. Koepke, Hannover). The data were reduced by the ZAF correction technique. All crystals proved to be homogeneous and, within error limits, of the same composition. Mean values of 94 point analyses are reported in Table 1 showing that the crystal-chemical constraints – (i) sum of positive valences = 8, (ii) sum of tetrahedral plus octahedral cations = 3 – are closely matched. Deviations from these constraints, all well within one standard deviation of the observed values, were accounted for following Ganguly *et al*. (1994).

High temperature experiments

Strategy

The structure refinements in this study are based on two groups of single-crystal X-ray intensity data sets that were collected on a conventional and a rotating anode diffractometer. These groups are referred to as (MS) and (BN), respectively. The (MS)-data were measured at ambient temperatures on crystals which had been equilibrated at 525 °C, 600 °C, 700 °C, and 900 °C, respectively, and then quenched to room temperature.

The (BN)-data sets, consisting of two subgroups, were collected *in situ* at elevated temperatures using a rotating anode diffractometer. The first subgroup (BN-HT) consisted of data measured between 600 °C and 900 °C in intervals of 50 °C. The temperature overlap with the equilibrium temperatures of the quenched crystals was deliberately chosen in order to test whether or not the respective Fe^{2+},Mg distributions had been frozen in without redistribution. This measure had been prompted by the results of Redfern *et al.* (2000) (Fig. 1) according to which the preservation of a cation equilibrium distribution upon quenching is unlikely for temperatures exceeding 500 °C. In that case, the site occupancies obtained from our *in situ* and *ex situ* measurements for one and the same equilibration temperature should disagree.

The second subgroup of BN-data (BN-LT) consisted of intensity data collected on crystals which had been quenched from equilibrium at the temperature of 600 °C. For comparison, on both diffractometers room temperature measurements were carried out. Then, full data sets were collected at 20 °C, 100 °C, 200 °C, 300 °C and finally 600 °C. One can safely assume that the state of order acquired at 600 °C will not change at temperatures of at most 300 °C, even over a two days data collection period (Aikawa *et al.*, 1985; Ottonello *et al.*, 1990). Therefore, these measurements were expected to provide structural results related to a distinct and fixed state of order and thus reflect pure thermal effects that are uncontaminated by a redistribution of Fe^{2+} and Mg. Details of the heating runs are compiled in Table 2.

Technical procedure

For the *in situ* experiments, the crystals were first fixed with silica wool inside silica glass capillaries of 0.3 mm diameter which were then evacuated to 10^{-5} mbar and filled with a CO/CO_2 gas mixture in several cycles, before sealing them off. The different gas mixtures provided oxygen fugacities that correspond to buffering with Fe/FeO within temperature intervals of about 200 °C. Thus, for the various temperature intervals, different gas mixtures were filled which in total covered the temperature range from 20 °C to 900 °C. The sample crystals were heated on the diffractometer by a hot nitrogen gas stream "containing" the primary beam. A detailed description of the heating device, its performance and in particular the method of temperature assessment is given by Scheufler *et al.* (1997).

For the annealing-and-quenching experiments, the crystals were also inserted into silica glass capillaries of 0.5 mm diameter. The capillaries were then placed into silica glass tubes which housed Fe/FeO mixtures separated from the capillaries by silica glass wool. Before sealing these tubes, they were filled in several cycles with purified Ar after evacuation to 10^{-5} mbar. At the end of the annealing experiments the silica capsules were quenched in water.

Data collection and reduction

The room temperature X-ray intensity data (MS) were collected on an ENRAF-NONIUS-CAD4 four-circle diffractometer using MoKα-radiation monochromatized by a pyrolytic graphite crystal. The data were measured up to $\sin(\theta)/\lambda = 1.08$ Å^{-1} in the octants hkl, $\overline{h}$kl, $\overline{h}\overline{k}$l, and h$\overline{k}$l using an ω-2θ scan mode optimized for each run. The *in situ* measurements (BN) were performed on a rotating Mo-anode diffractometer, RIGAKU AFC6, equally equipped with a graphite monochromator. Due to the gas stream heater the data collection was limited to $\sin(\theta)/\lambda = 0.70$ Å^{-1}, but intensities were measured for full spheres in all *in situ* experiments. The data reductions for the (MS)-CAD4-measurements were carried out with the program system MOLEN (ENRAF-NONIUS), the (BN)-data were reduced with REDUCE (Eichhorn, 1987a). Absorption effects were corrected by the semi-empirical method of North *et al.* (1968) in case of (MS) and by using ABSCOR (Eichhorn, 1987b) for the (BN)-data. After absorption correction, equivalent and multiple reflections were averaged, e.g. with RINTAN (Kirfel, 1993). More details about data collection and reduction procedures are summarized in Table 2.

Structure refinement

All structure refinements were carried out in space group *Pbnm* using the program RFINE 90, which is a version of RFINE4 updated by Finger & Prince (1975) and locally modified by R. Heinemann. Atomic scattering factors were taken from Cromer & Waber (1974) and Hovestreydt (1983), anomalous dispersion corrections from Doyle & Turner (1968). A partially ionic valence scheme was used. All atoms are considered fully ionized except for silicon (Si^{2+}) and oxygen ($O^{1.5-}$). The large Ca and Mn cations were assumed to occupy the M2 site. Fe^{2+} and Mg were free to fractionate between M1 and M2, subject to the site occupancy constraints

$$X_{Fe}^{M1} + X_{Mg}^{M1} = 1$$

$$X_{Fe}^{M2} + X_{Mg}^{M2} = 1 - X_{Ca}^{M2} - X_{Mn}^{M2}, \quad (1)$$

and the chemical constraint

$$X_{Fe}^{M1} + X_{Fe}^{M2} = 0.9351 \text{ (see Table 1).} \quad (2)$$

$X_{element}^{site}$ denotes the amount of Fe^{2+} or Mg occupying the M1 or M2 sites. The $|F_o|$ observations were weighted according to $w = [\sigma^2(F_o + (\frac{1}{2}R_i \cdot F_o)^2]^{-1}$ subject to the robust/resistant technique. R_i is the $|I_{obs}|$ based internal agreement of the data

Table 2. Thermal treatment of the samples, data collection and reduction parameters.

data set		annealing temperature [°C]	annealing time	type of measurement	max. $\sin\theta/\lambda$[Å^{-1}]	No. of unique refl.	internal R (ll)
MS	Bo- 2-1	as is	–	RT	1.09	1725	0.022
	2-2	600	7 d	*ex situ*	1.09	1722	0.020
	2-3	700	4 d	*ex situ*	1.09	1724	0.022
	Bo- 5-1	as is	–	RT	1.09	1727	0.032
	5-2	700	4 d	*ex situ*	1.09	1725	0.030
	5-3	525	22 d	*ex situ*	1.09	1727	0.037
	5-4	900	1 d	*ex situ*	1.09	1727	0.030
	Bo- 8-1	as is	–	RT	1.09	1725	0.019
	8-2	600	7 d	*ex situ*	1.09	1722	0.022
	8-3	700	4 d	*ex situ*	1.09	1725	0.022
	8-4	525	22 d	*ex situ*	1.09	1726	0.024
	8-5	900	1 d	*ex situ*	1.09	1725	0.022
BN	Bo-10-1	20	–	*in situ*	0.70	466	0.024
	10-2	104	–	*in situ*	0.70	466	0.024
	10-3	202	–	*in situ*	0.70	467	0.024
	10-4	306	–	*in situ*	0.70	471	0.024
	10-5	601	1 d	*in situ*	0.70	477	0.025
	10-6	656	1 d	*in situ*	0.70	477	0.026
	10-7	701	12 h	*in situ*	0.70	478	0.025
	10-8	753	12 h	*in situ*	0.70	480	0.025
	Bo- 2-4	748	6 h	*in situ*	0.70	479	0.025
	2-5	804	3 h	*in situ*	0.70	481	0.025
	2-6	852	16 h	*in situ*	0.70	482	0.024
	2-7	907	14 h	*in situ*	0.70	483	0.025

Note: *ex situ* = room temperature (RT) measurement after annealing and quenching

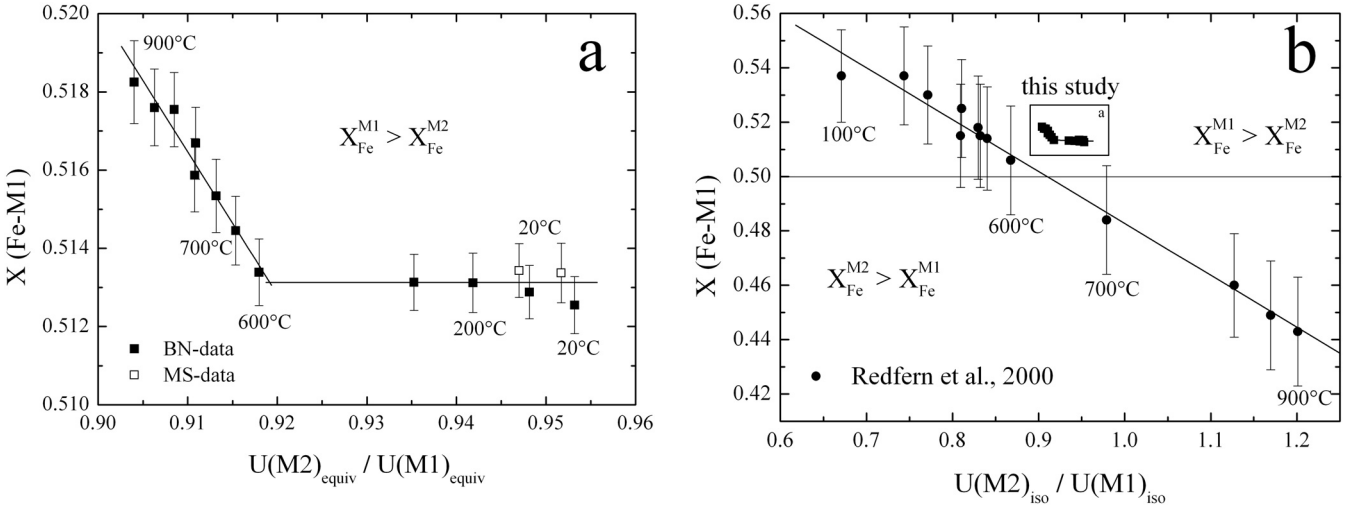

Fig. 2. Relation between site occupancy X_{Fe}^{M1} and ratio of atomic displacement parameters, U_{equiv}, at the M2 and M1 sites. (a) This study: values between 20 °C and 600 °C derive from crystals that were equilibrated at 600 °C, then quenched to room temperature and measured at T ≤ 600 °C. Therefore, between 20 °C and 600 °C X_{Fe}^{111} is expected to be constant within error limits. Data above 600 °C are from crystals equilibrated and then measured at the temperature of interest. (b) Redfern *et al*. (2000): The refined site occupancies display a pronounced correlation with the ratio of isotropic displacement parameters, U_{iso}, including the range between 100 °C and 600 °C X_{Fe}^{111}. Values increase with temperature contrary to our results (see insert). Note also the enormous difference in the spread of the site occupancy values and ratios of displacement parameters obtained in the two studies.

(e.g., Le Hénaff *et al.*, 1997). An extinction coefficient was refined according to Becker & Coppens (1974; type I isotropic extinction assuming a Lorentzian mosaic distribution). Because of its high correlation with the scale factor, this was done only in the final stages of the refinement.

Results and discussion

M-site order/anti-order

It is well known that in structure refinements site occupancies and atomic displacement parameters (ADP's) experi-

Table 3. Atomic fractional coordinates and anisotropic thermal displacement parameters [Å^2] obtained from refinements with *in situ* data (BN-data).

sample		Bo-10							
T [°C]		20	104	202	306	601	656	701	753
Si	x	0.42834 (10)	0.42843 (9)	0.42837 (10)	0.42844 (9)	0.42844 (11)	0.42838 (11)	0.42842 (12)	0.42861 (12)
	y	0.09578 (4)	0.09579 (4)	0.09586 (5)	0.09583 (4)	0.09585 (5)	0.09584 (5)	0.09588 (6)	0.09586 (6)
	U_{11}	0.0051 (2)	0.0057 (2)	0.0067 (2)	0.0073 (2)	0.0105 (2)	0.0111 (2)	0.0116 (3)	0.0123 (3)
	U_{22}	0.0068 (2)	0.0075 (2)	0.0087 (2)	0.0099 (2)	0.0146 (2)	0.0155 (2)	0.0166 (3)	0.0174 (3)
	U_{33}	0.0061 (2)	0.0073 (2)	0.0083 (2)	0.0097 (2)	0.0139 (2)	0.0148 (2)	0.0159 (3)	0.0168 (3)
	U_{12}	0.0001 (2)	0.0002 (2)	0.0003 (2)	0.0003 (2)	0.0002 (2)	0.0005 (2)	0.0005 (2)	0.0005 (2)
M1	X_{Fe}	0.5126 (7)	0.5129 (7)	0.5131 (8)	0.5131 (7)	0.5134 (9)	0.5145 (9)	0.5153 (9)	0.5159 (9)
	U_{11}	0.0062	0.0073	0.0087	0.0103	0.0157	0.0168	0.0177	0.0189
	U_{22}	0.0093	0.0111	0.0135	0.0164	0.0261	0.0282	0.0299	0.0321
	U_{33}	0.0063	0.0074	0.0089	0.0106	0.0167	0.0180	0.0191	0.0205
	U_{12}	0.0001	0.0001	0.0001	0.0001	–0.0001	–0.0002	–0.0002	–0.0003
	U_{13}	–0.0007	–0.0009	–0.0011	–0.0013	–0.0020	–0.0021	–0.0023	–0.0024
	U_{23}	–0.0015	–0.0019	–0.0022	–0.0027	–0.0039	–0.0041	–0.0043	–0.0046
M2	X_{Fe}	0.4225 (7)	0.4222 (7)	0.4220 (8)	0.4220 (7)	0.4217 (9)	0.4206 (9)	0.4198 (9)	0.4192 (9)
	x	0.98707 (7)	0.98716 (6)	0.98724 (7)	0.98743 (7)	0.98816 (9)	0.98824 (9)	0.98837 (10)	0.98847 (10)
	y	0.27884 (3)	0.27896 (3)	0.27911 (3)	0.27924 (3)	0.27963 (4)	0.27974 (4)	0.27985 (4)	0.27998 (4)
	U_{11}	0.0086	0.0099	0.0117	0.0137	0.0205	0.0220	0.0232	0.0247
	U_{22}	0.0060	0.0072	0.0087	0.0103	0.0155	0.0166	0.0175	0.0185
	U_{33}	0.0062	0.0074	0.0090	0.0109	0.0176	0.0190	0.0203	0.0218
	U_{12}	0.0004	0.0003	0.0003	0.0003	0.0004	0.0005	0.0005	0.0005
O1	x	0.7659 (2)	0.7660 (2)	0.7656 (3)	0.7652 (2)	0.7643 (3)	0.7637 (3)	0.7638 (3)	0.7637 (3)
	y	0.0922 (1)	0.0922 (1)	0.0924 (1)	0.0924 (1)	0.0925 (1)	0.0927 (1)	0.0926 (2)	0.0928 (2)
	U_{11}	0.0066 (5)	0.0069 (5)	0.0080 (5)	0.0082 (5)	0.0122 (6)	0.0122 (6)	0.0122 (7)	0.0128 (7)
	U_{22}	0.0097 (6)	0.0109 (5)	0.0133 (6)	0.0151 (6)	0.0226 (7)	0.0241 (8)	0.0267 (9)	0.0281 (9)
	U_{33}	0.0061 (5)	0.0080 (5)	0.0094 (6)	0.0113 (6)	0.0177 (7)	0.0190 (7)	0.0205 (8)	0.0216 (8)
	U_{12}	0.0001 (5)	0.0004 (5)	0.0002 (5)	0.0000 (5)	0.0002 (6)	0.0004 (6)	0.0007 (7)	0.0004 (7)
O2	x	0.2150 (2)	0.2153 (2)	0.2154 (3)	0.2153 (2)	0.2152 (3)	0.2152 (3)	0.2152 (3)	0.2152 (3)
	y	0.4504 (1)	0.4506 (1)	0.4507 (1)	0.4508 (1)	0.4515 (1)	0.4513 (1)	0.4515 (1)	0.4517 (1)
	U_{11}	0.0077 (5)	0.0088 (5)	0.0103 (6)	0.0117 (5)	0.0171 (7)	0.0182 (7)	0.0189 (8)	0.0199 (8)
	U_{22}	0.0069 (5)	0.0079 (5)	0.0090 (6)	0.0099 (5)	0.0151 (7)	0.0153 (7)	0.0162 (7)	0.0167 (7)
	U_{33}	0.0080 (6)	0.0089 (5)	0.0113 (6)	0.0132 (6)	0.0197 (7)	0.0216 (7)	0.0227 (8)	0.0235 (8)
	U_{12}	0.0000 (5)	–0.0003 (4)	0.0002 (5)	–0.0002 (5)	0.0005 (6)	–0.0002 (6)	0.0000 (7)	0.0002 (7)
O3	x	0.2830 (2)	0.2832 (1)	0.2836 (2)	0.2837 (2)	0.2844 (2)	0.2847 (2)	0.2849 (2)	0.2852 (2)
	y	0.1641 (1)	0.1641 (1)	0.1640 (1)	0.1641 (1)	0.1638 (1)	0.1638 (1)	0.1638 (1)	0.1637 (1)
	z	0.0352 (1)	0.0353 (1)	0.0356 (1)	0.0357 (1)	0.0364 (2)	0.0367 (2)	0.0370 (2)	0.0372 (2)
	U_{11}	0.0069 (4)	0.0082 (3)	0.0093 (4)	0.0111 (4)	0.0169 (5)	0.0178 (5)	0.0188 (5)	0.0204 (5)
	U_{22}	0.0089 (3)	0.0108 (3)	0.0131 (4)	0.0152 (4)	0.0221 (5)	0.0246 (5)	0.0257 (5)	0.0265 (5)
	U_{33}	0.0077 (4)	0.0087 (3)	0.0100 (4)	0.0117 (4)	0.0178 (5)	0.0190 (5)	0.0200 (5)	0.0204 (5)
	U_{12}	0.0004 (3)	0.0005 (3)	0.0007 (3)	0.0006 (3)	0.0009 (4)	0.0012 (4)	0.0012 (4)	0.0015 (4)
	U_{13}	0.0001 (3)	0.0000 (3)	–0.0003 (3)	–0.0002 (3)	–0.0008 (4)	–0.0006 (4)	–0.0007 (5)	–0.0007 (5)
	U_{23}	0.0016 (3)	0.0024 (3)	0.0027 (3)	0.0037 (3)	0.0056 (4)	0.0062 (4)	0.0061 (5)	0.0069 (5)

ence correlation effects. The correlation becomes evident when the ratio of site occupancies X_{Fe}^{M2}/X_{Fe}^{M1} is plotted against the ratio of equivalent displacement parameters $U(M2)_{equiv}$ / $U(M1)_{equiv}$ (e.g., Kroll *et al.*, 1997; Heinemann *et al.*, 1999, 2000). In order to judge whether the refined site occupancies possibly suffer from the correlation effect we have based our study on the *in situ* intensity data BN-LT collected between 20 °C and 600 °C on two crystals that had been equilibrated at 600 °C and then quenched. As noted above, the highest non-equilibrium temperature of measurement (300 °C) is not expected to have any effect on the quenched state of order. The obtained site occupancies were therefore expected to be the same within the temperature range 20 °C – 600 °C.

The refinements were performed as follows. First, all parameters including the site occupancies and anisotropic ADP's were varied simultaneously. A plot of the ADP's *versus* the temperature revealed regular changes from 20 °C up to 900 °C, though of course with some scatter. Since this scatter is expected to correlate with site occupancies, we have fitted least-squares second-order polynomials to the ADP values and then in order to avoid correlations taken the fit curves to calculate ADP's that were used as fixed input to the final refinements. This measure yielded practically con-

Table 3 (cont.)

sample		Bo-2			
T [°C]		748	804	852	907
Si	x	0.42858 (11)	0.42858 (11)	0.42863 (12)	0.42865 (13)
	y	0.09594 (5)	0.09596 (5)	0.09596 (5)	0.09598 (6)
	U_{11}	0.0120 (2)	0.0127 (2)	0.0128 (2)	0.0138 (3)
	U_{22}	0.0165 (2)	0.0175 (2)	0.0183 (2)	0.0194 (3)
	U_{33}	0.0170 (2)	0.0182 (3)	0.0190 (3)	0.0200 (3)
	U_{12}	0.0003 (2)	0.0005 (2)	0.0004 (2)	0.0005 (2)
M1	X_{Fe}	0.5167 (9)	0.5175 (9)	0.5176 (10)	0.5182 (11)
	U_{11}	0.0188	0.0200	0.0212	0.0225
	U_{22}	0.0319	0.0342	0.0364	0.0388
	U_{33}	0.0203	0.0218	0.0232	0.0248
	U_{12}	–0.0003	–0.0003	–0.0004	–0.0004
	U_{13}	–0.0024	–0.0025	–0.0026	–0.0028
	U_{23}	–0.0045	–0.0048	–0.0050	–0.0053
M2	X_{Fe}	0.4184 (9)	0.4176 (9)	0.4175 (10)	0.4169 (11)
	x	0.98853 (9)	0.98871 (9)	0.98886 (10)	0.98907 (11)
	y	0.27992 (4)	0.28002 (4)	0.28014 (4)	0.28025 (5)
	U_{11}	0.0246	0.0262	0.0277	0.0294
	U_{22}	0.0184	0.0196	0.0206	0.0218
	U_{33}	0.0216	0.0233	0.0248	0.0266
	U_{12}	0.0005	0.0006	0.0006	0.0006
O1	x	0.7640 (3)	0.7637 (3)	0.7634 (3)	0.7632 (3)
	y	0.0928 (1)	0.0928 (1)	0.0928 (1)	0.0928 (2)
	U_{11}	0.0133 (6)	0.0141 (6)	0.0140 (7)	0.0160 (7)
	U_{22}	0.0269 (7)	0.0286 (8)	0.0301 (8)	0.0320 (9)
	U_{33}	0.0220 (7)	0.0234 (8)	0.0248 (8)	0.0259 (9)
	U_{12}	0.0006 (6)	0.0005 (6)	0.0005 (7)	0.0003 (7)
O2	x	0.2150 (3)	0.2149 (3)	0.2151 (3)	0.2151 (3)
	y	0.4517 (1)	0.4518 (1)	0.4520 (1)	0.4522 (1)
	U_{11}	0.0202 (7)	0.0216 (7)	0.0227 (7)	0.0238 (8)
	U_{22}	0.0163 (6)	0.0169 (7)	0.0173 (7)	0.0184 (7)
	U_{33}	0.0230 (8)	0.0249 (8)	0.0266 (8)	0.0286 (9)
	U_{12}	0.0001 (6)	0.0002 (6)	–0.0002 (6)	0.0004 (7)
O3	x	0.2853 (2)	0.2856 (2)	0.2859 (2)	0.2861 (2)
	y	0.1638 (1)	0.1638 (1)	0.1637 (1)	0.1638 (1)
	z	0.0369 (2)	0.0371 (2)	0.0374 (2)	0.0374 (2)
	U_{11}	0.0203 (5)	0.0215 (5)	0.0230 (5)	0.0245 (6)
	U_{22}	0.0261 (5)	0.0280 (5)	0.0296 (5)	0.0312 (6)
	U_{33}	0.0212 (5)	0.0224 (5)	0.0235 (5)	0.0248 (6)
	U_{12}	0.0010 (4)	0.0015 (4)	0.0014 (4)	0.0016 (5)
	U_{13}	–0.0007 (4)	–0.0005 (4)	–0.0006 (5)	–0.0009 (5)
	U_{23}	0.0066 (4)	0.0069 (5)	0.0077 (5)	0.0078 (5)

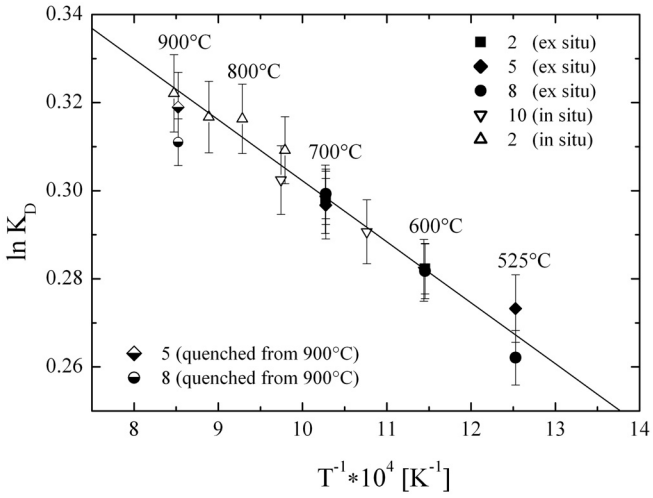

Fig. 3. Variation of $\ln K_D$ (Table 5) with inverse temperature. Data measured *in situ* and *ex situ* agree except for samples quenched from 900 °C. Weighted regression analysis omitting the 900 °C data yields $\ln K_D = 0.4422(\pm 0.0070)) - 140.0(\pm 6.5) / T\ (K)$.

stant values of X_{Fe}^{M2} between 20 °C and 600 °C (Tab. 3 and 5, Fig. 2a), thus giving credit to the assumption that the site occupancies obtained between 600 °C and 900 °C are also unaffected by correlation effects.

Figure 2a shows that at 600 °C Fe^{2+} is enriched in the M1 site and that it fractionates further into this site as temperature is raised. As noted in the introduction, this result agrees with recently obtained *ex situ* data of Morozov *et al.* (2001, 2005), but is at variance with the *in situ* data of Redfern *et al.* (2000) (Fig. 1). Figure 2b compares site occupancies and isotropic displacement parameters obtained by Redfern *et al*. (2000) with our data (see insert), all measured *in situ* within the same temperature range. The two studies yield incompatible results. The variation of the ratio of the U_{iso}'s is much larger in the study of Redfern *et al.* as applies also to the changes in the X_{Fe}^{M1} values. According to Redfern *et al.* X_{Fe}^{M1} strongly decreases with temperature whereas we find it just slightly increasing. In addition, Redfern *et al.* report a crossover from anti-order, $X_{Fe}^{M1} > X_{Fe}^{M2}$, to order, $X_{Fe}^{M2} > X_{Fe}^{M1}$, not far from the temperature at which $U(M2)_{iso}$ exceeds $U(M1)_{iso}$, also at variance with our results.

Quenching experiments

The results of Morozov *et al.* (2001, 2005) and of our study not only disagree with Redfern *et al.* (2000) with respect to the site preferences, but also with respect to the implications derived from Fig. 1 concerning the blocking temperature for Fe^{2+},Mg redistribution during quenching. The samples used by Morozov *et al.* have been quenched to room temperature within a few seconds (Brinkmann, 2000). No redistribution effect appears in the regular increase of Fe^{2+} in M1 between 500 °C and 800 °C. Assumed, the site occupancies of Redfern *et al.* are correct, noticeable redistribution must have continued down to a temperature of about 500 °C.

As described above, nine data sets have been collected on crystals first equilibrated at 525 °C, 600 °C, 700 °C and 900 °C, respectively, and then quenched (Tables 4 and 5). As is apparent from Fig. 3, no difference between *in situ* and *ex situ* site occupancies is observed up to 700 °C.

Only the two crystals quenched from 900 °C show in fact some redistribution corresponding to an average apparent equilibrium temperature $T_{ae} = 825 \pm 60$ °C as can be seen from Fig. 3. Accordingly, at the chosen quench speed, site occupancies can be recovered from temperatures at least as high as about 750 °C. Therefore, if in the starting sample of Redfern *et al.* (2000), Fe^{2+} was in fact enriched in M2, it should be still so after the quench, corresponding to a freezing temperature of about 750 °C (their quench was some-

Table 4. Atomic fractional coordinates and anisotropic thermal displacement parameters [Å^2] obtained from refinements with *ex situ* data (MS-data).

sample		Bo-2			Bo-5			
T [°C]		as is	600	700	as is	525	700	900
Si	x	0.42829 (3)	0.42834 (4)	0.42834 (4)	0.42833 (5)	0.42837 (5)	0.42840 (5)	0.42838 (6)
	y	0.09575 (2)	0.09577 (2)	0.09580 (2)	0.09574 (3)	0.09578 (2)	0.09583 (3)	0.09580 (3)
	U_{11}	0.00339 (5)	0.00407 (6)	0.00411 (5)	0.00408 (8)	0.00429 (8)	0.00459 (8)	0.00442 (8)
	U_{22}	0.00505 (5)	0.00557 (6)	0.00538 (5)	0.00580 (8)	0.00591 (8)	0.00588 (8)	0.00607 (9)
	U_{33}	0.00537 (6)	0.00528 (6)	0.00543 (6)	0.00561 (9)	0.00565 (8)	0.00583 (8)	0.00597 (9)
	U_{12}	0.00032 (4)	0.00032 (5)	0.00028 (4)	0.00029 (7)	0.00038 (6)	0.00019 (7)	0.00030 (7)
M1	X_{Fe}	0.5046 (6)	0.5134 (7)	0.5153 (6)	0.5085 (9)	0.5123 (9)	0.5152 (9)	0.5179 (10)
	U_{11}	0.00468 (4)	0.00534 (4)	0.00540 (4)	0.00549 (6)	0.00557 (5)	0.00573 (6)	0.00571 (6)
	U_{22}	0.00764 (4)	0.00827 (5)	0.00811 (4)	0.00856 (6)	0.00846 (6)	0.00861 (6)	0.00873 (7)
	U_{33}	0.00573 (4)	0.00567 (4)	0.00578 (4)	0.00587 (6)	0.00618 (6)	0.00615 (6)	0.00627 (6)
	U_{12}	0.00001 (3)	0.00006 (4)	–0.00004 (3)	–0.00004 (5)	0.00007 (4)	–0.00004 (5)	0.00007 (5)
	U_{13}	–0.00069 (3)	–0.00070 (4)	–0.00072 (3)	–0.00068 (5)	–0.00068 (5)	–0.00068 (5)	–0.00071 (5)
	U_{23}	–0.00140 (3)	–0.00140 (3)	–0.00141 (3)	–0.00134 (5)	–0.00143 (4)	–0.00141 (5)	–0.00139 (5)
M2	X_{Fe}	0.4305 (6)	0.4217 (7)	0.4198 (6)	0.4266 (9)	0.4228 (9)	0.4199 (9)	0.4172 (10)
	x	0.98671 (3)	0.98671 (3)	0.98673 (3)	0.98672 (4)	0.98674 (4)	0.98673 (4)	0.98679 (4)
	y	0.27884 (1)	0.27885 (1)	0.27884 (1)	0.27883 (2)	0.27883 (2)	0.27883 (2)	0.27886 (2)
	U_{11}	0.00667 (4)	0.00727 (5)	0.00736 (5)	0.00736 (7)	0.00743 (7)	0.00772 (7)	0.00754 (8)
	U_{22}	0.00485 (4)	0.00528 (4)	0.00517 (4)	0.00551 (6)	0.00550 (6)	0.00569 (6)	0.00565 (7)
	U_{33}	0.00585 (4)	0.00572 (5)	0.00591 (4)	0.00601 (6)	0.00620 (6)	0.00611 (6)	0.00625 (7)
	U_{12}	0.00012 (3)	0.00018 (4)	0.00013 (3)	0.00011 (5)	0.00015 (5)	0.00009 (6)	0.00008 (6)
O1	x	0.76627 (8)	0.76615 (10)	0.76614 (9)	0.76613 (13)	0.76624 (13)	0.76609 (13)	0.76592 (14)
	y	0.09204 (5)	0.09214 (5)	0.09212 (5)	0.09204 (7)	0.09214 (7)	0.09206 (7)	0.09214 (7)
	U_{11}	0.00362 (11)	0.00430 (14)	0.00441 (12)	0.00428 (18)	0.00446 (17)	0.00472 (19)	0.00464 (20)
	U_{22}	0.00891 (14)	0.00927 (16)	0.00927 (15)	0.00957 (23)	0.00942 (21)	0.00968 (23)	0.01004 (25)
	U_{33}	0.00688 (14)	0.00691 (15)	0.00692 (14)	0.00680 (21)	0.00720 (19)	0.00704 (20)	0.00707 (21)
	U_{12}	0.00055 (11)	0.00039 (12)	0.00047 (11)	0.00044 (17)	0.00032 (16)	0.00045 (18)	0.00045 (19)
O2	x	0.21521 (9)	0.21494 (11)	0.21512 (10)	0.21522 (14)	0.21509 (14)	0.21511 (14)	0.21493 (15)
	y	0.45025 (4)	0.45025 (5)	0.45021 (4)	0.45024 (6)	0.45032 (6)	0.45041 (6)	0.45033 (7)
	U_{11}	0.00651 (12)	0.00731 (15)	0.00725 (13)	0.00723 (20)	0.00725 (19)	0.00745 (20)	0.00758 (22)
	U_{22}	0.00491 (12)	0.00525 (14)	0.00532 (13)	0.00551 (19)	0.00563 (18)	0.00578 (20)	0.00579 (21)
	U_{33}	0.00781 (14)	0.00762 (15)	0.00780 (14)	0.00815 (22)	0.00792 (20)	0.00830 (21)	0.00828 (22)
	U_{12}	–0.00018 (11)	–0.00014 (12)	–0.00015 (11)	0.00010 (17)	0.00008 (16)	–0.00002 (18)	–0.00015 (19)
O3	x	0.28278 (6)	0.28282 (7)	0.28278 (6)	0.28270 (10)	0.28291 (9)	0.28298 (9)	0.28289 (10)
	y	0.16425 (3)	0.16428 (3)	0.16429 (3)	0.16421 (5)	0.16421 (4)	0.16423 (5)	0.16433 (5)
	z	0.03493 (5)	0.03490 (6)	0.03493 (6)	0.03498 (8)	0.03496 (8)	0.03497 (8)	0.03502 (8)
	U_{11}	0.00618 (9)	0.00672 (10)	0.00684 (9)	0.00672 (14)	0.00696 (13)	0.00715 (14)	0.00705 (15)
	U_{22}	0.00827 (9)	0.00869 (11)	0.00870 (10)	0.00880 (14)	0.00889 (13)	0.00921 (15)	0.00922 (16)
	U_{33}	0.00698 (10)	0.00700 (10)	0.00705 (10)	0.00695 (14)	0.00731 (14)	0.00732 (14)	0.00748 (15)
	U_{12}	0.00059 (8)	0.00052 (9)	0.00046 (8)	0.00054 (13)	0.00041 (12)	0.00049 (13)	0.00061 (14)
	U_{13}	–0.00031 (8)	–0.00031 (9)	–0.00032 (8)	–0.00028 (12)	–0.00039 (11)	–0.00037 (12)	–0.00052 (12)
	U_{23}	0.00243 (8)	0.00247 (9)	0.00231 (9)	0.00237 (13)	0.00251 (12)	0.00236 (13)	0.00246 (13)

what slower than ours). However, the authors find Fe^{2+} enriched in M1 indicating a freezing temperature of about 500 °C, which is much too low (Fig. 1).

Temperature variation of $\ln K_D$ in related transition metal-Mg olivines

It is most instructive to relate the temperature dependence of $\ln K_D = \ln(X_{Fe}^{M1} X_{Mg}^{M2} / X_{Fe}^{M2} X_{Mg}^{M1})$ in FeMg olivine to the $\ln K_D$ relations known from other transition metal-Mg olivines. Figure 4a shows $\ln K_D$ values for three temperatures calculated on the basis of data reported for MnMg olivine (Redfern *et al*., 1997), CoMg olivine (Sutanto, 2004; Sutanto *et al*., 2004) and NiMg olivine (Henderson *et al*., 2001) and plotted against the respective numbers of 3d-electrons of the transition metals. Choosing these numbers is arbitrary in the sense that one could likewise use the numbers of paired electrons, magnetic moments, cation radii or any other parameter related to the configuration of the 3d-shells. Second order polynomials fitted to the data points show a common intersection close to the six 3d-electrons of Fe. This result gives credit to the $\ln K_D$ data used, and it predicts that for FeMg olivine $\ln K_D$ obtains small and positive values at all temperatures. It also conforms to the general observation that natural olivines are always close to disorder, i.e. with

Table 4 (cont.)

sample		Bo-8				
T [°C]		as is	525	600	700	900
Si	x	0.42830 (4)	0.42825 (4)	0.42834 (4)	0.42831 (4)	0.42835 (3)
	y	0.09574 (2)	0.09578 (2)	0.09578 (2)	0.09578 (2)	0.09582 (2)
	U_{11}	0.00311 (5)	0.00350 (6)	0.00334 (6)	0.00321 (5)	0.00352 (5)
	U_{22}	0.00600 (6)	0.00538 (6)	0.00596 (7)	0.00573 (6)	0.00603 (5)
	U_{33}	0.00534 (5)	0.00544 (6)	0.00572 (6)	0.00561 (6)	0.00580 (5)
	U_{12}	0.00028 (4)	0.00032 (5)	0.00028 (5)	0.00029 (4)	0.00030 (4)
M1	X_{Fe}	0.5069 (7)	0.5110 (8)	0.5134 (8)	0.5155 (7)	0.5169 (6)
	U_{11}	0.00444 (4)	0.00480 (4)	0.00471 (4)	0.00457 (4)	0.00486 (4)
	U_{22}	0.00869 (4)	0.00813 (5)	0.00875 (5)	0.00846 (4)	0.00877 (4)
	U_{33}	0.00570 (4)	0.00575 (4)	0.00605 (5)	0.00601 (4)	0.00619 (4)
	U_{12}	–0.00004 (3)	–0.00002 (3)	–0.00005 (4)	–0.00003 (3)	–0.00002 (3)
	U_{13}	–0.00071 (3)	–0.00067 (3)	–0.00069 (4)	–0.00066 (3)	–0.00070 (3)
	U_{23}	–0.00138 (3)	–0.00138 (3)	–0.00138 (3)	–0.00139 (3)	–0.00140 (3)
M2	X_{Fe}	0.4282 (7)	0.4241 (8)	0.4217 (8)	0.4196 (7)	0.4182 (6)
	x	0.98669 (3)	0.98667 (3)	0.98666 (3)	0.98671 (3)	0.98675 (3)
	y	0.27882 (1)	0.27883 (1)	0.27884 (1)	0.27883 (1)	0.27884 (1)
	U_{11}	0.00641 (5)	0.00673 (5)	0.00662 (5)	0.00650 (5)	0.00678 (4)
	U_{22}	0.00574 (4)	0.00524 (4)	0.00576 (5)	0.00547 (4)	0.00577 (4)
	U_{33}	0.00585 (4)	0.00597 (5)	0.00619 (5)	0.00616 (4)	0.00636 (4)
	U_{12}	0.00012 (3)	0.00018 (4)	0.00016 (4)	0.00013 (3)	0.00015 (3)
O1	x	0.76617 (9)	0.76621 (10)	0.76625 (10)	0.76628 (9)	0.76610 (8)
	y	0.09208 (5)	0.09206 (5)	0.09212 (5)	0.09210 (5)	0.09221 (4)
	U_{11}	0.00332 (12)	0.00378 (13)	0.00363 (13)	0.00337 (12)	0.00384 (11)
	U_{22}	0.00995 (15)	0.00929 (16)	0.00986 (18)	0.00951 (15)	0.00987 (14)
	U_{33}	0.00692 (13)	0.00692 (14)	0.00709 (15)	0.00725 (14)	0.00733 (13)
	U_{12}	0.00039 (11)	0.00029 (12)	0.00048 (13)	0.00034 (11)	0.00039 (10)
O2	x	0.21524 (9)	0.21529 (10)	0.21510 (11)	0.21511 (10)	0.21501 (9)
	y	0.45013 (4)	0.45022 (4)	0.45020 (5)	0.45025 (4)	0.45026 (4)
	U_{11}	0.00641 (13)	0.00666 (14)	0.00669 (15)	0.00646 (13)	0.00679 (12)
	U_{22}	0.00565 (13)	0.00523 (13)	0.00572 (15)	0.00543 (13)	0.00593 (12)
	U_{33}	0.00779 (14)	0.00757 (15)	0.00788 (15)	0.00805 (14)	0.00812 (13)
	U_{12}	–0.00014 (11)	–0.00010 (12)	–0.00010 (13)	–0.00010 (11)	–0.00013 (10)
O3	x	0.28267 (6)	0.28271 (7)	0.28276 (7)	0.28283 (7)	0.28277 (6)
	y	0.16425 (3)	0.16428 (3)	0.16428 (4)	0.16429 (3)	0.16430 (3)
	z	0.03483 (5)	0.03484 (6)	0.03489 (6)	0.03479 (6)	0.03491 (5)
	U_{11}	0.00591 (9)	0.00619 (10)	0.00616 (10)	0.00594 (9)	0.00615 (8)
	U_{22}	0.00920 (10)	0.00862 (10)	0.00910 (11)	0.00887 (10)	0.00921 (9)
	U_{33}	0.00695 (9)	0.00705 (10)	0.00718 (10)	0.00726 (10)	0.00731 (9)
	U_{12}	0.00061 (8)	0.00046 (9)	0.00054 (9)	0.00045 (8)	0.00055 (8)
	U_{13}	–0.00031 (8)	–0.00043 (8)	–0.00031 (9)	–0.00033 (8)	–0.00039 (7)
	U_{23}	0.00240 (8)	0.00232 (9)	0.00243 (9)	0.00238 (9)	0.00226 (8)

little variation in K_D. Small and positive $\ln K_D$ values at all temperatures are in fact observed in this study, in contrast to Redfern *et al.* (2000), see Fig. 4b. At 1050 °C, their $\ln K_D$ value exhibits a significant deviation from the intersection of the curves. Thus, since our observations smoothly fit a picture established by the 'neighbouring' transition metal-Mg olivines, whereas those of Redfern et al (2000) do not, there is strong evidence that the latter are questionable.

Unit-cell dimensions

The unit-cell dimensions are listed in Table 6. Their relative changes with temperature are plotted in Fig. 5. All parameters increase smoothly. The little redistribution of Fe^{2+} and Mg which sets in above 600 °C generates a hardly detectable effect. Only the observed volumes plot somewhat below the (dashed) extrapolation of a second-order polynomial fitted to the data between 20 °C and 600 °C, indicating that anti-order which increases above 600 °C reduces the cell volume. This behaviour agrees with the general prediction by Hazen & Navrotsky (1996) that a disordered phase has a larger volume than its ordered equivalent. Pressure can hence be expected to promote anti-order in (Fe,Mg) olivine. Observations on the ordering behaviour of NiMg olivine at high pressure made by Chen *et al.* (1996) and evaluated by Henderson *et al.* (2001) confirm this expectation.

As a consequence of fitting the cell dimensions by second-order polynomials, the linear thermal expansion coeffi-

Table 5. Agreement factors (%), site occupancies and distribution coefficients.

data set		T (°C)	N_{hkl}	R	R_W	GoF	X_{Fe}^{M1}	X_{Fe}^{M2}	K_D	$\ln K_D$
MS	Bo-2-1	as is	1453	1.46	1.31	0.82	0.5046 (6)	0.4305 (6)	1.233	0.209 (5)
	2-2	600	1423	1.54	1.41	0.85	0.5134 (7)	0.4217 (7)	1.326	0.282 (6)
	2-3	700	1439	1.44	1.32	0.81	0.5153 (6)	0.4198 (6)	1.347	0.298 (5)
	Bo-5-1	as is	1307	1.96	1.84	0.79	0.5085 (9)	0.4266 (9)	1.273	0.242 (8)
	5-2	700	1302	1.85	1.71	0.79	0.5152 (9)	0.4199 (9)	1.345	0.297 (8)
	5-3	525	1330	1.80	1.82	0.76	0.5123 (9)	0.4228 (9)	1.314	0.273 (8)
	5-4	900	1289	1.93	1.76	0.80	0.5179 (10)	0.4172 (10)	1.376	0.319 (8)
	Bo-8-1	as is	1522	1.61	1.48	0.95	0.5069 (7)	0.4282 (7)	1.257	0.229 (6)
	8-2	600	1496	1.74	1.65	0.94	0.5134 (8)	0.4217 (8)	1.326	0.282 (6)
	8-3	700	1494	1.58	1.49	0.90	0.5155 (7)	0.4196 (7)	1.349	0.299 (6)
	8-4	525	1485	1.65	1.61	0.90	0.5110 (8)	0.4241 (8)	1.300	0.262 (6)
	8-5	900	1502	1.42	1.41	0.88	0.5169 (6)	0.4182 (6)	1.365	0.311 (5)
BN	Bo-10-1	20	343	1.15	1.18	0.85	0.5126 (7)	0.4225 (7)	1.317	0.275 (6)
	10-2	104	347	1.11	1.07	0.82	0.5129 (7)	0.4222 (7)	1.320	0.278 (6)
	10-3	202	345	1.22	1.22	0.86	0.5131 (8)	0.4220 (8)	1.323	0.280 (6)
	10-4	306	347	1.21	1.11	0.82	0.5131 (7)	0.4220 (7)	1.323	0.280 (6)
	10-5	601	345	1.37	1.35	0.87	0.5134 (9)	0.4217 (9)	1.326	0.282 (7)
	10-6	656	342	1.41	1.40	0.87	0.5145 (9)	0.4206 (9)	1.337	0.291 (7)
	10-7	701	340	1.50	1.47	0.90	0.5153 (9)	0.4198 (9)	1.347	0.298 (8)
	10-8	753	345	1.55	1.49	0.90	0.5159 (9)	0.4192 (9)	1.353	0.302 (8)
	Bo-2-4	748	359	1.48	1.62	1.03	0.5167 (9)	0.4184 (9)	1.362	0.309 (8)
	2-5	804	365	1.52	1.70	1.04	0.5175 (9)	0.4176 (9)	1.372	0.316 (8)
	2-6	852	364	1.61	1.73	1.05	0.5176 (10)	0.4175 (10)	1.373	0.317 (8)
	2-7	907	365	1.80	1.89	1.09	0.5182 (11)	0.4169 (11)	1.380	0.322 (9)

$X_{Mg}^{M1} = 1 - X_{Fe}^{M1}$, $X_{Mg}^{M2} = 1 - X_{Ca}^{M2} - X_{Mn}^{M2} - X_{Fe}^{M2}$, $K_D = X_{Fe}^{M1} \cdot X_{Mg}^{M2} / X_{Fe}^{M2} \cdot X_{Mg}^{M1}$

$$R = \frac{\Sigma(|F_o - F_c|)}{\Sigma(F_o)} \qquad R_W = \left(\frac{\Sigma w \cdot (F_o - F_c)^2}{\Sigma w \cdot F_o^2}\right)^{1/2} \qquad GoF = \left(\frac{\Sigma w \cdot (F_o - F_c)^2}{N_{hkl} - P)}\right)^{1/2} = \text{goodness of fit.}$$

N_{hkl}= number of reflections, P = number of independent parameters, (N_{hkl} – P = degrees of freedom. For annealing temperatures, annealing times and type of measurement see Table 2.

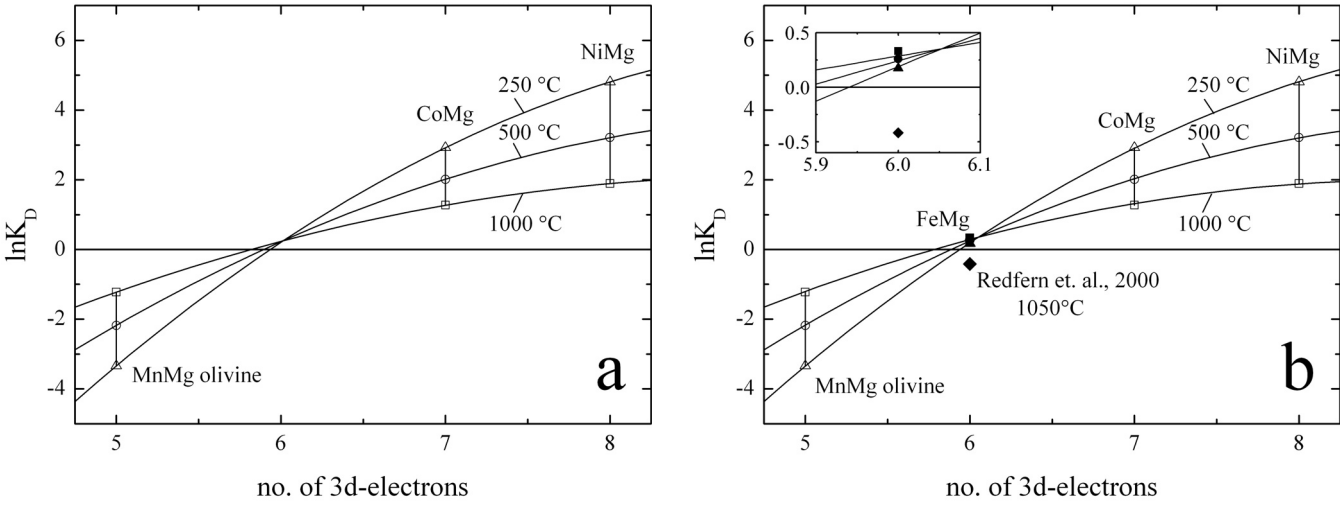

Fig. 4. (a) Variation with temperature of $\ln K_D$ calculated for MnMg (Redfern *et al.*, 1997), CoMg (Sutanto, 2004) and NiMg olivine (Henderson *et al.*, 2001), plotted versus the number of 3d-electrons of the respective transition metal cation. The curves have been fitted only to the data points of MnMg, CoMg and NiMg olivine and predict that FeMg olivine should be anti-ordered with small variations at all temperatures. (b) As (a) including results of Redfern *et al*. (2000) and the present study.

cients $\alpha_T = 1/x_T (dx/dT)$, where $x = a$, b, c and V, increase linearly in the temperature ranges below and above 600 °C, respectively. The onset of the anti-ordering is indicated by small off-sets (Fig. 6).

Octahedral distances

In a structure refinement, the M-O distances can be determined more accurately than the site occupancies and the

Table 6. Unit-cell dimensions [Å] and volumes [Å^3].

sample	T [°C]	*a*	*b*	*c*	*V*
Bo-10	20	4.7942 (12)	10.3500 (17)	6.0436 (8)	299.88 (10)
10	104	4.7961 (12)	10.3557 (17)	6.0479 (8)	300.38 (10)
10	202	4.7996 (10)	10.3652 (15)	6.0543 (8)	301.20 (9)
10	306	4.8043 (9)	10.3779 (15)	6.0630 (8)	302.29 (8)
10	601	4.8181 (8)	10.4158 (15)	6.0884 (6)	305.54 (7)
10	656	4.8209 (8)	10.4230 (16)	6.0927 (7)	306.16 (8)
10	701	4.8231 (8)	10.4296 (15)	6.0963 (8)	306.66 (8)
10	753	4.8270 (8)	10.4381 (15)	6.1023 (8)	307.46 (8)
Bo-2	748	4.8257 (6)	10.4373 (16)	6.1009 (7)	307.28 (7)
2	804	4.8291 (7)	10.4433 (18)	6.1058 (8)	307.92 (8)
2	852	4.8325 (7)	10.4552 (18)	6.1128 (8)	308.85 (8)
2	907	4.8358 (8)	10.4636 (17)	6.1176 (8)	309.55 (8)

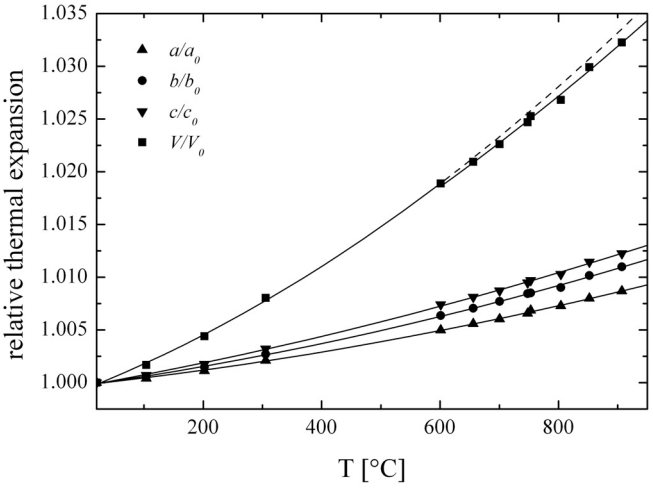

Fig. 5. Variation with temperature of cell dimensions and volume relative to their values at 20 °C. The dashed curve is extrapolated from a second-order polynomial fit to the volume data between 20 °C and 600 °C. The onset of anti-ordering at 600 °C causes a slight reduction of the volume.

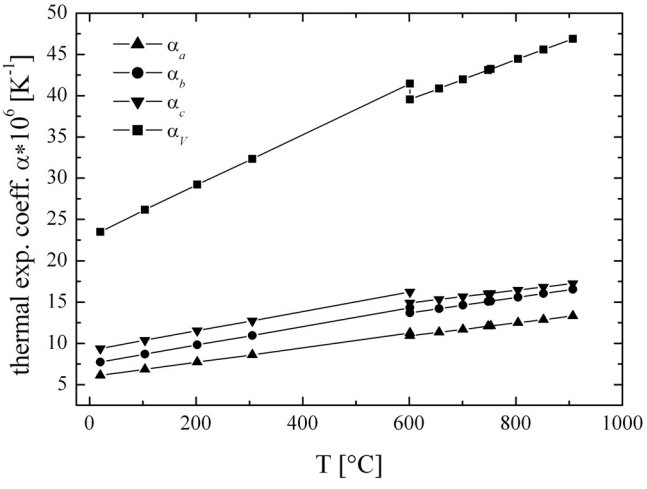

Fig. 6. Variation with temperature of the thermal expansion coefficients $\alpha_T = 1/x_T\,(dx/dT)$, where $x = a$, b, c and V.

atomic displacement parameters. Accordingly, we can expect that the mean distances, <M-O>, acquired in this study (Table 7) agree within error limits with those of Redfern *et al.* (2000). This is in fact seen to be approximately true comparing their figure 4 with our Fig. 7. Second-order polynomial fits to the data points obtained between 20 °C and 600 °C were extrapolated to 900 °C (dashed curves). While the measured <M2-O> distances plot somewhat below the extrapolated part of the curve, the <M1-O> distances plot above. Similar to the volume behaviour, this can be interpreted as a consequence of the Fe^{2+},Mg redistribution which sets in at 600 °C. Since Fe^{2+}, with the larger ionic radius, increasingly fractionates into M1, the coordination octahedron expands in excess of a mere thermal expansion. Concomitantly, the expansion of the M2 octahedron slows down. The data of Redfern *et al.* (2000) reveal a similar behaviour. However, since the authors found Fe^{2+} to increase in M2 with temperature, the ionic radius argument contradicted the relative decrease of the <M2-O> distances. As a consequence, the authors argued that the thermal expansion of the Fe-O bond is less than that of the Mg-O bond. This being true, the effect is small compared to the antagonistic effect of the ionic size as evidenced by the comparative studies of Smyth (1975) and Lager & Meagher (1978).

In addition to the results presented in Fig. 4, the relations between the <M-O> distances and the isotropic cation thermal displacement parameters depicted in Fig. 8 are another keystone to giving more credit to the present results than to the findings of Redfern *et al.* (2000). Since these relations are not explicitly dependent on temperature they are most helpful in judging whether or not our U_{equiv} and hence also the refined site occupancies are reasonable.

For the type of structures discussed here, it is generally agreed that the strength of a given bond is positively correlated with its bond length and that the stronger a bond the smaller the isotropic displacements of the bonded atoms. This expectation is perfectly met by our data, but not by those of Redfern *et al.* (2000). According to their results there exist two <M-O> regions with unexplained significantly different slopes $d(<M\text{-}O>)/d(U_{iso})$ [A^{-1}] implying drastic changes in the binding forces between the cations and the oxygen atoms. For M1, U(M1) becomes much less dependent on <M-O> whereas for M2, U(M2) becomes

Table 7. Bond lengths [Å] and ensuing octahedral length distortions.

sample	Bo-10							
T [°C]	20	104	202	306	601	656	701	753
Si-O1 [1][a]	1.6187 (13)	1.6193 (12)	1.6187 (13)	1.6185 (12)	1.6188 (15)	1.6170 (15)	1.6180 (16)	1.6180 (16)
Si-O2 [1]	1.6538 (13)	1.6536 (12)	1.6556 (13)	1.6563 (12)	1.6555 (15)	1.6577 (15)	1.6578 (16)	1.6567 (16)
Si-O3 [2]	1.6346 (9)	1.6347 (8)	1.6332 (9)	1.6348 (8)	1.6352 (10)	1.6340 (11)	1.6327 (11)	1.6335 (11)
<Si-O>	1.6357 (12)	1.6359 (11)	1.6358 (12)	1.6365 (11)	1.6365 (14)	1.6362 (14)	1.6362 (15)	1.6361 (15)
M1-O1 [2]	2.1101 (8)	2.1113 (8)	2.1151 (9)	2.1185 (8)	2.1294 (10)	2.1331 (10)	2.1339 (11)	2.1367 (11)
M1-O2 [2]	2.1008 (8)	2.1006 (8)	2.1021 (9)	2.1045 (8)	2.1108 (10)	2.1124 (10)	2.1132 (11)	2.1145 (11)
M1-O3 [2]	2.1843 (8)	2.1862 (8)	2.1886 (8)	2.1915 (8)	2.1995 (10)	2.2018 (10)	2.2038 (11)	2.2061 (11)
<M1-O>	2.1317 (8)	2.1327 (8)	2.1353 (9)	2.1382 (8)	2.1466 (10)	2.1491 (10)	2.1503 (11)	2.1524 (11)
M2-O1 [1]	2.2040 (12)	2.2059 (11)	2.2088 (13)	2.2138 (12)	2.2274 (15)	2.2301 (15)	2.2332 (16)	2.2350 (16)
M2-O2 [1]	2.0851 (12)	2.0874 (11)	2.0882 (13)	2.0899 (12)	2.0976 (14)	2.0967 (15)	2.0979 (16)	2.1006 (16)
M2-O3a [2]	2.0678 (8)	2.0692 (8)	2.0720 (9)	2.0752 (8)	2.0860 (10)	2.0882 (10)	2.0906 (11)	2.0926 (11)
M2-O3b [2]	2.2601 (9)	2.2619 (8)	2.2649 (9)	2.2675 (8)	2.2769 (10)	2.2787 (11)	2.2797 (10)	2.2825 (12)
<M2-O>	2.1575 (10)	2.1593 (9)	2.1618 (11)	2.1649 (10)	2.1751 (12)	2.1768 (12)	2.1786 (13)	2.1810 (13)
D (M1-O) [b]	0.01753	0.01786	0.01784	0.01784	0.01779	0.01778	0.01803	0.01813
D (M1-O)$_n$ [c]	0.98635	1.00484	1.00370	1.00389	1.00125	1.00056	1.01444	1.02004
D (M2-O)	0.03994	0.03994	0.04007	0.04008	0.03997	0.04010	0.03994	0.03998
D (M2-O)$_n$	0.99848	0.99857	1.00166	1.00190	0.99919	1.00259	0.99845	0.99946

sample	Bo-2			
T [°C]	748	804	852	907
Si-O1 [1][a]	1.6189 (15)	1.6187 (16)	1.6183 (16)	1.6181 (18)
Si-O2 [1]	1.6574 (15)	1.6573 (15)	1.6575 (15)	1.6577 (17)
Si-O3 [2]	1.6343 (11)	1.6336 (11)	1.6330 (12)	1.6339 (13)
<Si-O>	1.6369 (14)	1.6365 (14)	1.6363 (14)	1.6366 (16)
M1-O1 [2]	2.1358 (10)	2.1382 (11)	2.1410 (11)	2.1432 (12)
M1-O2 [2]	2.1148 (10)	2.1165 (10)	2.1170 (11)	2.1183 (11)
M1-O3 [2]	2.2068 (10)	2.2090 (10)	2.2116 (11)	2.2144 (12)
<M1-O>	2.1525 (10)	2.1546 (10)	2.1565 (11)	2.1586 (12)
M2-O1 [1]	2.2335 (16)	2.2366 (16)	2.2410 (16)	2.2451 (18)
M2-O2 [1]	2.0996 (14)	2.1001 (15)	2.1037 (15)	2.1051 (17)
M2-O3a [2]	2.0905 (11)	2.0928 (11)	2.0960 (11)	2.0970 (13)
M2-O3b [2]	2.2823 (11)	2.2841 (11)	2.2869 (12)	2.2893 (13)
<M2-O>	2.1798 (12)	2.1818 (13)	2.1851 (13)	2.1871 (15)
D (M1-O) [b]	0.01829	0.01833	0.01862	0.01886
D (M1-O)$_n$ [c]	1.02915	1.03160	1.04776	1.06161
D (M2-O)	0.04029	0.04033	0.04023	0.04056
D (M2-O)$_n$	1.00724	1.00822	1.00564	1.01397

[a] bracketed numbers denote multiplicities
[b] $D(M_{1,2}\text{-O}) = \{\Sigma [(M_{1,2}\text{-O})_i - \langle M_{1,2}\text{-O}\rangle]^2 / n\}^{1/2} / \langle M_{1,2}\text{-O}\rangle$
[c] $D(M_{1,2}\text{-O})_n = D(M_{1,2}\text{-O})_T / D(M_{1,2}\text{-O})_{RT}$

much more sensitive to changes in <M-O>. In other words, redistributing only a few percent Mg and Fe (at most about 7%) is supposed to significantly change the average chemical bonding of the cations. This is highly improbable in view of all crystal-chemical knowledge. Similar effects in orthopyroxenes exhibiting much larger ordering effects are not known. Therefore, and since it is known from experience that the refinement of reliable atomic displacement parameters from powder data is more difficult than from single-crystal data we strongly suspect that the U_{iso} reported by Redfern *et al.* (2000) as well as the correlated site occupancies are compromised by the correlation effect.

Octahedral distortions

Sizes and distortions of the coordination octahedra are factors that influence intracrystalline cation partitioning. Various distortion parameters have been suggested of which the angular variance and the quadratic elongation (Robinson *et al.*, 1971) are most popular. Depending on which measure of distortion is chosen, the M1 or the M2 octahedron in the olivine structure is the more distorted one. We have used relative standard deviations of bond lengths and angles defined as

$$D_p = \frac{\sqrt{\Sigma(p_j - \bar{p})^2 / n}}{\bar{p}} \qquad (3)$$

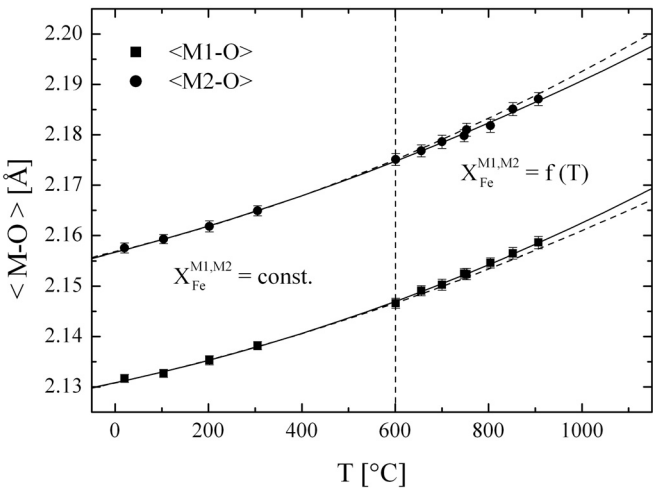

Fig. 7. Variation with temperature of the mean octahedral distances < M1-O> and <M2-O>. The dashed curves are extrapolated from second-order polynomial fits to the data points between 20 °C and 600 °C. Note that the migration of the larger ion Fe^{2+} from M2 to M1 at T > 600 °C is reflected by the simultaneous decrease of <M2-O> and increase of <M1-O>.

Table 8. Bond angles [°] and ensuing octahedral angular distortions.

sample	Bo-10							
T [°C]	20	104	202	306	601	656	701	753
O1-T-O2 [1][(a)]	113.22 (6)	113.31 (6)	113.34 (7)	113.37 (6)	113.48 (8)	113.51 (8)	113.49 (8)	113.63 (9)
O1-T-O3 [2]	115.87 (4)	115.84 (4)	115.80 (4)	115.79 (4)	115.69 (5)	115.64 (5)	115.66 (5)	115.63 (5)
O2-T-O3 [2]	102.50 (4)	102.48 (4)	102.48 (4)	102.49 (4)	102.46 (5)	102.52 (5)	102.52 (5)	102.49 (5)
O3-T-O3 [1]	105.18 (6)	105.19 (6)	105.26 (6)	105.24 (6)	105.38 (7)	105.37 (8)	105.34 (8)	105.33 (8)
<O-T-O>	109.19 (5)	109.20 (5)	109.22 (5)	109.22 (5)	109.25 (6)	109.26 (6)	109.25 (7)	109.27 (7)
O1-M1-O2 [2]	86.64 (4)	86.57 (3)	86.60 (4)	86.59 (3)	86.54 (4)	86.61 (4)	86.57 (4)	86.55 (4)
O1-M1-O2' [2]	93.36 (4)	93.43 (3)	93.40 (4)	93.41 (3)	93.47 (4)	93.39 (4)	93.42 (4)	93.45 (4)
O1-M1-O3 [2]	84.79 (4)	84.77 (4)	84.76 (4)	84.77 (4)	84.79 (5)	84.80 (5)	84.77 (5)	84.75 (5)
O1-M1-O3' [2]	95.21 (4)	95.23 (4)	95.24 (4)	95.23 (4)	95.21 (5)	95.20 (5)	95.23 (5)	95.25 (5)
O2-M1-O3 [2]	106.50 (4)	106.56 (4)	106.62 (4)	106.66 (4)	106.97 (4)	106.99 (5)	107.07 (5)	107.17 (5)
O2-M1-O3' [2]	73.50 (4)	73.44 (4)	73.38 (4)	73.34 (4)	73.03 (4)	73.01 (5)	72.93 (5)	72.83 (5)
<O-M2-O>	90.00 (4)	90.00 (3)	90.00 (4)	90.00 (4)	90.00 (4)	90.00 (4)	90.00 (5)	90.00 (5)
O1-M2-O3 [2]	80.88 (3)	80.85 (3)	80.85 (4)	80.84 (3)	80.78 (4)	80.83 (4)	80.78 (4)	80.78 (4)
O1-M2-O3'' [2]	91.29 (3)	91.28 (3)	91.25 (3)	91.20 (3)	91.11 (3)	91.06 (4)	91.05 (4)	91.02 (4)
O2-M2-O3 [2]	96.81 (4)	96.82 (3)	96.85 (4)	96.91 (4)	97.19 (4)	97.19 (4)	97.23 (5)	97.29 (5)
O2-M2-O3''' [2]	90.28 (3)	90.30 (3)	90.30 (3)	90.32 (3)	90.25 (4)	90.27 (4)	90.28 (4)	90.27 (4)
O3-M2-O3' [1]	70.13 (4)	70.07 (4)	69.93 (4)	69.90 (4)	69.66 (5)	69.54 (5)	69.43 (6)	69.36 (6)
O3-M2-O3'' [2]	88.18 (2)	88.15 (2)	88.15 (2)	88.13 (2)	88.12 (2)	88.12 (2)	88.12 (3)	88.11 (3)
O3-M2-O3''' [1]	112.90 (5)	113.00 (4)	113.14 (5)	113.20 (5)	113.42 (6)	113.54 (6)	113.65 (6)	113.73 (6)
<O-M2-O>	90.07 (4)	90.07 (3)	90.07 (4)	90.07 (3)	90.08 (4)	90.08 (4)	90.08 (5)	90.08 (5)
D (θ_{M1}) [(b)]	0.11308	0.11355	0.11392	0.11416	0.11603	0.11603	0.11662	0.11730
D (θ_{M1})$_n$ [(c)]	1.00002	1.00415	1.00747	1.00955	1.02611	1.02609	1.03131	1.03735
D θ_{M2})	0.11052	0.11090	0.11149	0.11177	0.11310	0.11349	0.11407	0.11444
D (θ_{M2})$_n$	1.00002	1.00347	1.00876	1.01128	1.02332	1.02685	1.03211	1.03543

Table 8 (cont.)

sample	Bo-2			
T [°C]	748	804	852	907
O1-T-O2 [1][(a)]	113.55 (8)	113.55 (8)	113.62 (8)	113.62 (9)
O1-T-O3 [2]	115.59 (5)	115.56 (5)	115.54 (5)	115.51 (6)
O2-T-O3 [2]	102.54 (5)	102.56 (5)	102.53 (5)	102.54 (6)
O3-T-O3 [1]	105.41 (8)	105.43 (8)	105.46 (8)	105.50 (9)
<O-T-O>	109.27 (6)	109.27 (7)	109.29 (7)	109.29 (8)
O1-M1-O2 [2]	86.55 (4)	86.57 (4)	86.52 (4)	86.52 (5)
O1-M1-O2' [2]	93.45 (4)	93.43 (4)	93.48 (4)	93.48 (5)
O1-M1-O3 [2]	84.75 (5)	84.76 (5)	84.77 (5)	84.81 (6)
O1-M1-O3' [2]	95.25 (5)	95.24 (5)	95.23 (5)	95.19 (6)
O2-M1-O3 [2]	107.13 (5)	107.21 (5)	107.30 (5)	107.35 (5)
O2-M1-O3' [2]	72.87 (5)	72.79 (5)	72.70 (5)	72.65 (5)
<O-M2-O>	90.00 (4)	90.00 (5)	90.00 (5)	90.00 (5)
O1-M2-O3 [2]	80.80 (4)	80.82 (4)	80.79 (4)	80.80 (5)
O1-M2-O3'' [2]	91.03 (4)	90.99 (4)	90.98 (4)	90.94 (4)
O2-M2-O3 [2]	97.28 (4)	97.32 (4)	97.38 (5)	97.42 (5)
O2-M2-O3''' [2]	90.26 (4)	90.25 (4)	90.24 (4)	90.25 (4)
O3-M2-O3' [1]	69.46 (5)	69.37 (6)	69.25 (6)	69.24 (6)
O3-M2-O3'' [2]	88.08 (2)	88.07 (3)	88.08 (3)	88.05 (3)
O3-M2-O3''' [1]	113.70 (6)	113.79 (6)	113.91 (6)	113.95 (7)
<O-M2-O>	90.09 (4)	90.09 (5)	90.09 (5)	90.09 (5)
D (θ_{M1}) [(b)]	0.11702	0.11750	0.11810	0.11827
D (θ_{M1})$_n$ [(c)]	1.03486	1.03906	1.04437	1.04591
D θ_{M2})	0.11415	0.11453	0.11510	0.11525
D (θ_{M2})$_n$	1.03289	1.03628	1.04141	1.04282

[(a)] bracketed numbers denote multiplicities

[(b)] $\theta_{M1,2}$ = (O–$M_{1,2}$–O) angle, $D(\theta_{M1,2}) = \{\Sigma [(\theta_{M1,2})_i - <\theta_{M1,2}>]^2 / n\}^{1/2} / <\theta_{M1,2}>$

[(c)] $D(\theta_{M1,2})_n = D(\theta_{M1,2})_T / D(\theta_{M1,2})_{RT}$

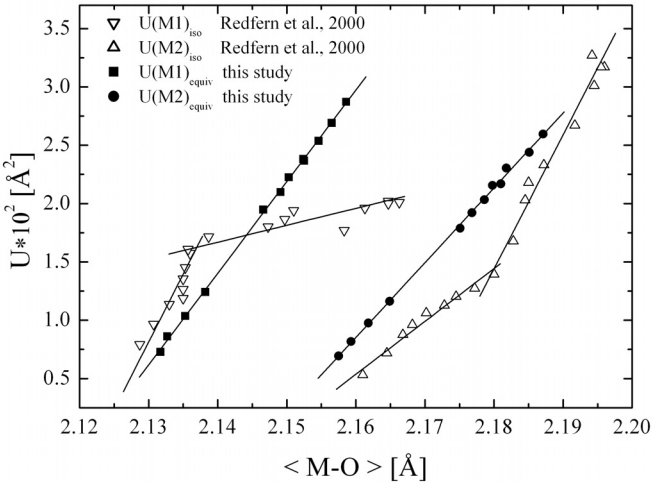

Fig. 8. Relation between the mean octahedral distances, <M1-O> and <M2-O>, and the respective isotropic atomic displacement parameters obtained by Redfern *et al.* (2000) and in this study.

where p_j are O-M1,2-O angles and M1,2-O distances, respectively. Bond angles and distortion parameters are given in Tables 7 and 8. The variations with temperature of the relative distortions are plotted in Fig. 9. With respect to the bond lengths the M2 octahedron is more than twice as distorted as the M1 octahedron, and both distortions vary little with temperature. Since the M1 cation is located on a centre of symmetry, interatomic forces acting on the cation cannot change its position. The M2 atom, on the other hand, is located on a mirror plane so that it is free to move in two direc-

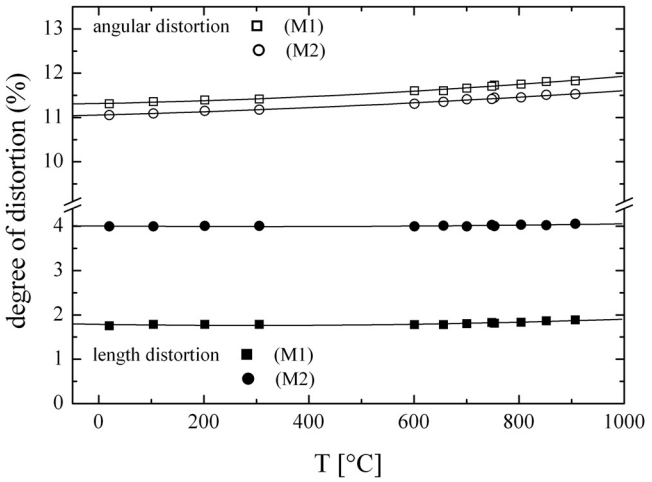

Fig. 9. Variation with temperature of length and angle distortion parameters D_p defined as normalized standard deviations $D_p = (\sqrt{\Sigma (p_j - \bar{p})^2 / n}) / \bar{p}$, where p are octahedral bond lengths and angles, respectively.

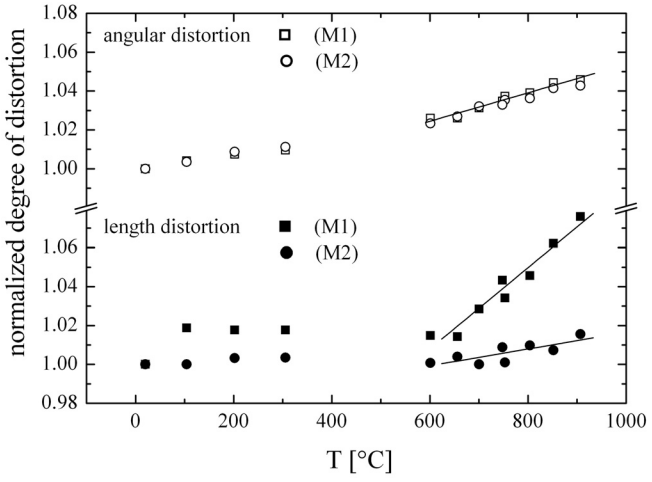

Fig. 10. Variation with temperature of distortion parameters relative to their values at 20 °C.

tions and interactions across edges shared between the M2 octahedron and three neighbouring polyhedra can become effective. Consequently, the M2-O bond length variation is larger than the M1-O bond length variation.

Compared to the relative bond length distortions the relative angular distortions are much larger, but very similar for M1 and M2. They clearly increase with temperature, with the M1 distortion increasing more than that of M2. Thus, the approximately hexagonal closed-packing of the oxygen atoms becomes less ideal with increasing temperature, as already noted by Brown & Prewitt (1973). The M1 octahedron shares two edges with neighbouring SiO_4 tetrahedra; the M2 octahedron shares only one. Since the (Fe,Mg)-Si interactions across the shared edges cause the largest deviations from the ideal 90° octahedral angles it is only natural that the M1 octahedron exhibits the larger angular distortion. The increase of the distortions with temperature is also a consequence of the edge sharing with tetrahedra. Tetrahedral bond lengths and angles are hardly sensitive to temperature changes (Brown, 1980; also see Tables 7 and 8). Therefore, for (Fe,Mg)-Si distances increasing with temperature, the angular distortions must necessarily also increase, and this more for the M1 than the M2 octahedron.

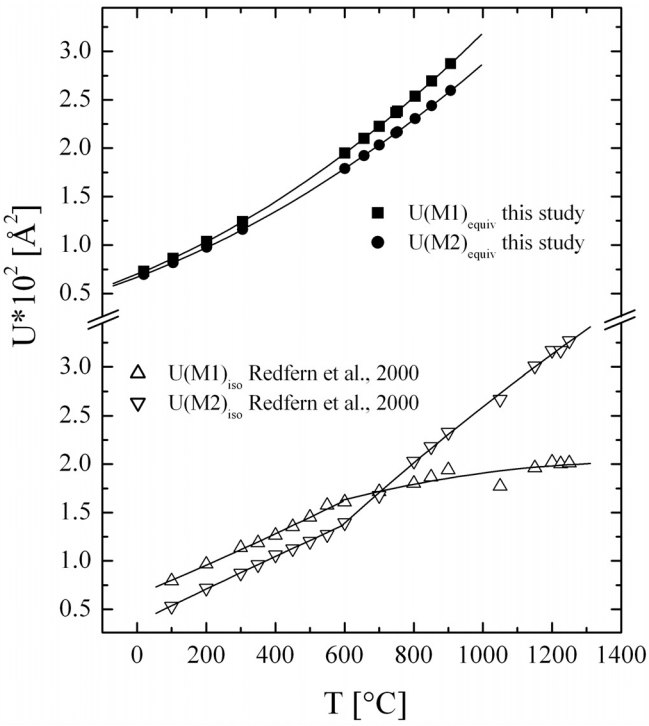

Fig. 11. Variation with temperature of the isotropic atomic displacement parameters obtained by Redfern *et al*. (2000) and in this study.

Figure 9 is not fit to reveal an effect that the Fe^{2+},Mg redistribution may have on the octahedral distortion. In Fig. 10 we have therefore plotted the distortion parameters normalized to their values at 20 °C. This shows that from 20 °C to 600 °C where pure thermal expansion is effective the relative distortions do hardly change relative to each another. At 600 °C, however, when the cation redistribution sets in, all four distortion parameters start to significantly increase, in a very similar way for M2, but quite differently for M1, for which the distortion in terms of bond lengths increases at a much higher rate than that in terms of angles. This ascribed to anti-ordering it appears that vice versa an increasing disorder is accompanied by a decreasing distortion, a general behaviour in agreement with expectation.

Atomic displacement parameters

The variation with temperature of the (equivalent) isotropic displacement parameters (Fig. 11) agrees with earlier findings by Brown & Prewitt (1973). At all temperatures, $U(M1)_{equiv}$ is larger than $U(M2)_{equiv}$, both without indication for an abrupt change of slope as apparent in the data of Redfern *et al*. (2000). The M1 atom, however, does not only "vibrate" with a larger amplitude, but also is the anisotropy of its thermal motion more pronounced and increasing with temperature than that of the M2 atom (Fig. 12a,b). This behaviour is probably related to the larger angular distortion

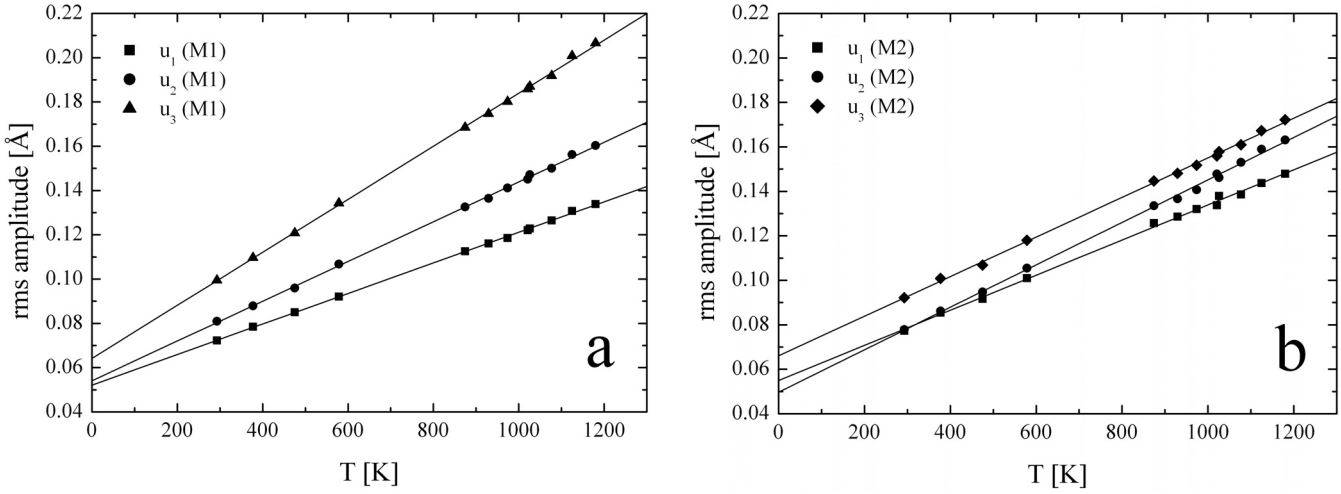

Fig. 12. Variation with temperature of the atomic root-mean-square (rms) amplitudes of apparent vibration at (a) the M1 and (b) the M2 octahedral site.

and to the reduction from cubic to approximately tetragonal site symmetry of the M1 octahedron.

Olivine geospeedometry

When a system that is capable of order-disorder reactions cools down from high temperatures the ordering process eventually freezes in at a state that depends on the cooling rate, which conversely can be inferred from the acquired state of order (Ganguly, 1982; Kroll *et al*., 1997). For the olivine mineral group Henderson *et al.* (1996) and Redfern *et al.* (1996) have shown that (Mn,Mg) and (Mn,Fe) olivines represent useful geospeedometers. Consequently the question has been repeatedly raised whether this may also apply to (Fe,Mg) olivines.

Compared to the MnMg olivine speedometer the variation of $\ln K_D$ with temperature is very small in FeMg olivine. Although the variation increases somewhat as the Fa content decreases (Heinemann *et al.*, 1999) (Fe,Mg) olivine will always stay inferior to other cation speedometers with regard to the magnitude of the ordering effect. On the other hand, (Fe,Mg) olivine could provide distinct advantages. (i) Compared to orthopyroxenes the chemical composition is much less contaminated by impurity species. (ii) The fast Fe^{2+},Mg exchange kinetics would allow for a better resolution of fast cooling events and for following slow cooling down to lower temperatures. However, besides of the inherent difficulties of accurate site occupancy determinations, the physical influences that govern the exchange kinetics and equilibrium states have to be better understood before a possible establishment of (Fe,Mg) olivine as a geospeedometer.

With these restrictions and caveats in mind we have performed an ordering path calculation for Fa48 based on the site occupancies determined on the untreated crystals Bo-2, 5, and 8 (Table 5). Our aim was to learn whether the obtained cooling rate would at least be reasonable. To simulate the ordering path we apply the Mueller (1967, 1969) rate equation as given by Kroll (2003),

$$\frac{dQ(t)}{dt} = -k_{21}\,[A \cdot \Delta Q + B \cdot (\Delta Q)^2] \qquad (4)$$

where

$$Q = \overline{X}^{M2}_{Fe} - \overline{X}^{M1}_{Fe}$$
$$\overline{X}^{M2}_{Fe} = X^{M2}_{Fe} / (X^{M2}_{Fe} + X^{M2}_{Mg})$$
$$\overline{X}^{M1}_{Fe} = X^{M1}_{Fe} / (X^{M1}_{Fe} + X^{M1}_{Mg})$$
$$\Delta Q = Q(t) - Q_{equilibrium}.$$

A and B depend on both the Fa content and the distribution coefficient K_D. k_{21} is the rate constant for the microscopic disordering step in the reaction

$$Fe^{M2} + Mg^{M1} \rightleftharpoons Fe^{M1} + Mg^{M2}. \qquad (5)$$

The progress of ordering during cooling of the host rock can be simulated when the temperature dependences of both K_D and k_{21} are known. $K_D(T)$ is obtained from a weighted regression of the data displayed in Fig. 3 (omitting the two quenches from 900 °C),

$$\ln K_D = 0.4422\ (\pm 0.0070) - 140.0\ (\pm 6.5)/T\ (K) \qquad (6)$$

Based on earlier work by Bocquet *et al.* (1983), Akamatsu & Kumazawa (1993) and Ganguly & Tazzoli (1994), Heinemann *et al.* (1999) derived for the rate constant of the Fe^{2+},Mg site exchange process

$$k_{21} = \frac{2\,\tilde{D}_b}{(b/4)^2}\left(\frac{K_D}{1 + K_D}\right), \qquad (7)$$

where b denotes the length of the *b* cell edge and $\tilde{D}_b$ is the coefficient of the Fe^{2+},Mg interdiffusion along *b*.

Chakraborty (1997) determined $\tilde{D}_c$ on olivine Fa14 which can be converted to $\tilde{D}_b$ from $\tilde{D}_b = \tilde{D}_c / 5$ (Heinemann *et al.*, 1999). The variation of $\tilde{D}_b$ with temperature obeys the Arrhenius relation,

$$\tilde{D}_b = \tilde{D}_c /5 = [\tilde{D}_0 \exp (-E_a / RT)] / 5 \quad (8)$$

where $\tilde{D}_0$ denotes the frequency factor and E_a the activation energy, both measured for diffusion along *c*. R is the gas constant. $\tilde{D}_0$ and E_a are functions of the Fa content (Buening & Buseck, 1973) so that the values of Chakraborty (1997) had to be recalculated for $X_{Fa} = 0.48$,

$$\ln \tilde{D}_0[m^2 / d] = -7.674 - 5.01(X_{Fa} - 0.14) \text{ at } f_{O_2} = 10^{-12} \text{ bar} \quad (9)$$

$$E_a[J/mol] = 226000 - 91661(X_{Fa} - 0.14). \quad (10)$$

$\tilde{D}_0$ also depends on the oxygen fugacity, $f_{O_2}(T)$ (Buening & Buseck, 1973),

$$\ln \tilde{D}_0(f_{O_2}) = \ln \tilde{D}_0(f_{O_2} = 10^{-12}\text{bar}) + 0.167 \ln \left(\frac{f_{O_2}(T)}{10^{-12}} \right). \quad (11)$$

Following Chakraborty (1997) we assume that in the pure extrinsic diffusion regime at low temperatures (roughly below 800 °C, pers. comm.) diffusion rates become independent of the oxygen fugacity because in that temperature regime the majority of point defects is provided by impurity defects. Using equation (11) we corrected the frequency factor $\tilde{D}_0$ to conform to an oxygen fugacity provided by the Fe/FeO buffer at 800 °C. Then, the temperature dependence of $\tilde{D}_b$ can be obtained from equation (8) and allows for calculating the Arrhenius parameters of the rate constant, k_{21}, according to equation (7),

$$k_{21} [d^{-1}] = 2.33 \cdot 10^{13} \exp \{-46.67[kJ/mol]/RT\}. \quad (12)$$

Finally, we assume that the temperature of the host rock drops according to

$$1/T = 1/T_0 + \eta t \quad (13)$$

where $T_0 = 800$ °C, t is time and η is a cooling constant. In the simulation of the ordering path, η was varied until the average site occupancy of the untreated crystals was reproduced. This resulted in an apparent equilibrium temperature $T_{ae} = 365$ °C and a cooling rate of -23 °C/y close to T_{ae}. Considering that we are dealing with a volcanic rock these results do not appear unreasonable and as such they confirm our earlier assumption that the *in situ* heating of crystals at 300 °C over a two day period does not change their state of order. They also support that a redistribution of Fe^{2+} and Mg during fast laboratory quenching will not be effective down to temperatures as low as 500 °C as would be necessary to explain the results of Redfern *et al.* (2000) (Fig. 1).

Conclusion

Since long, determinations of the Fe^{2+},Mg distributions in olivine delivered puzzling results. Kirfel (1996) performed a round robin in which a number of laboratories was asked to refine Fe^{2+},Mg site occupancies of orthopyroxene and olivine on the basis of given X-ray intensity data. The large spread of returned results was disconcerting. Fe^{2+} in olivine was reported either to be enriched in M1 or concentrated in M2 or randomly distributed over both sites. Princivalle (1990) reported a similar scatter obtained on olivines from mantle xenoliths, although all of them had the same thermal history. A likely explanation of the wide range of results appears to be the correlation between the refined site occupancies and the atomic displacement parameters. Therefore, we have paid special attention to this problem. The comparison of our $\ln K_D$ *vs.* 1/T relation with those of other transition metal-Mg olivines confirms the expectation that our data are not compromised (Fig. 4a,b). The slight enrichment of Fe^{2+} in M1 and the small variation of $\ln K_D$ with temperature, both being predicted by Fig. 4a, agree with the results of our refinements. More confirmation is provided by the Möß-bauer work of Morozov *et al.* (2001, 2005) the results of which with certainty do not suffer from the correlation effect. We therefore strongly suspect that although the atomic coordinates obtained in the refinements of Redfern *et al.* (2000) are essentially correct the reported site occupancies and atomic displacement parameters are not. The enormous differences between their results and ours, seen in Fig. 2b, imply that at least for small order-disorder effects the correlation can be much more harmful to the determination of reliable site occupancies than presumed so far.

Acknowledgements: This work was supported by grants given by the Deutsche Forschungsgemeinschaft to Herbert Kroll and Armin Kirfel which is gratefully acknowledged. Our thanks are also due to Dr. Fedora Martignago, Padova, Italy, who kindly donated the olivine bearing rock sample, and to Dr. Jürgen Koepke, Hannover, who provided careful electron microprobe analyses. The authors acknowledge careful reviews by two anonymous referees.

References

Aikawa, N., Kumazawa, M., Tokonami, M. (1985): Temperature dependence of intersite distribution of Mg and Fe in olivine and the associated change of lattice parameters. *Phys. Chem. Minerals*, **12**, 1–8.

Akamatsu, T. & Kumazawa, M. (1993): Kinetics of intracrystalline cation redistribution in olivine and its implication. *Phys. Chem. Minerals*, **19**, 423–430.

Artioli, G., Rinaldi, R., Wilson, C., Zanazzi, P.F. (1995): High-temperature Fe-Mg cation partitioning in olivine: *In situ* single-crystal neutron diffraction study. *Am. Mineral.*, **80**, 197–200.

Becker, P.J. & Coppens, P. (1974): Extinction within the limit of validity of the Darwin transfer equations. I. General formalism for primary and secondary extinction and their application to spherical crystals. *Acta Cryst.*, **A30**, 129–147.

Bocquet, J.L., Brébec, G., Limoge, Y. (1983): Diffusion in metals

and alloys. *in* R.W. Cahn & P. Haasen, Eds., Physical Metallurgy (3rd edition), p. 385–475. North-Holland Physics Publishing, Amsterdam.

Brinkmann, C. (2000): Untersuchung der Fe^{2+},Mg-Verteilung in synthetischen Olivinen mit IR-Spektroskopie. Diplomarbeit, Westfälische Wilhelms-Universität Münster, 126 pp.

Brotzu, P., Morbidelli, L., Piccirillo, E.M., Traversa, G. (1980): Volcanological and magmatological evidences of Boseti Complex (Main Ethiopian Rift). *in* "Geodynamic Evolution of the Afro-Arabic Rift System". Atti dei Convegni dei Lincei. Acc. *Naz. Dei Lincei 4*, **47**, 317–366.

Brown, G.E. Jr (1980): Olivines and silicate spinels. *in* Orthosilicates. Reviews in Mineralogy, Vol. 5, Mineralogical Society of America.

Brown, G.E. Jr & Prewitt, C.T. (1973): High temperature crystal chemistry of hortonolite. *Am. Mineral.*, **58**, 577–587.

Buening, D.K. & Buseck, P.R. (1973): Fe-Mg lattice diffusion in olivine. *Journ. Geophys. Research*, **78**, 6852–6862.

Chakraborty, S. (1997): Rates and mechanisms of Fe-Mg interdiffusion in olivine at 980–1300 °C. *Journ. Geophys. Res.*, **102**, 12317–12331.

Chen, J., Li, R., Parise, J.B., Weidner, D.J. (1996): Pressure-induced ordering in $(Ni,Mg)_2SiO_4$ olivine. *Am. Mineral.*, **81**, 1519–1522.

Cromer, D.T. & Waber, J.T. (1974): Atomic scattering factors for X-rays. *in* International tables for X-ray crystallography, Vol. IV, J.A. Ibers and W.A. Hamilton, eds., Kynoch, Birmingham.

Doyle, P.A. & Turner, P.S. (1968): Relativistic Hartree-Fock X-ray and electron scattering factors. *Acta Cryst.*, **A24**, 390–397.

Eichhorn, K. (1987a): REDUCE. Program for data reduction of step-scan measured reflection profiles of both neutron and X-rays. HASYLAB/DESY, Hamburg, Germany. Unpublished.

– (1987b): ABSCOR. Absorption correction of four-circle diffractometer data. Revised and updated from Coppens (1968). HASYLAB/DESY, Hamburg, Germany. Unpublished.

Finger, L.W. & Prince, E. (1975): A system of FORTRAN IV computer programs for crystal structural computations. *NBS Tech. Note*, 854.

Freiheit V., Heinemann R., Kroll H., Krane H.-G., Kirfel A. (2000) Thermal history of natural olivines from the temperature dependent cation distribution determined by laboratory and synchroton radiation X-ray diffraction. HASYLAB Annual Report 2000.

Ganguly, J. (1982): Mg-Fe order-disorder in ferromagnesian silicates. II. Thermodynamics, kinetics, and geological implications. *in* Advances in Physical Geochemistry, Vol. 2, S.K. Saxena, ed., Springer, New York, 58–99.

Ganguly, J. & Tazzoli, V. (1994): Fe^{2+}-Mg interdiffusion in orthopyroxene: retrieval from the data on intracrystalline exchange reaction. *Am. Mineral.*, **79**, 930–937.

Ganguly, J., Yang, H., Ghose, S. (1994): Thermal history of mesosiderites: Quantitative constraints from compositional zoning and Fe-Mg ordering in orthopyroxenes. *Geochim. Cosmochim. Acta*, **58**, 2711–2723.

Hazen, R.M. & Navrotsky, A. (1996): Effects of pressure on order-disorder reactions. *Am. Mineral.*, **81**, 1021–1035.

Heinemann, R., Staack, V., Fischer, A., Kroll, H., Vad, Th., Kirfel, A. (1999): Temperature dependence of Fe,Mg partitioning in Acapulco olivine. *Am. Mineral.*, **84**, 1400–1405.

Heinemann, R., Kroll, H., Langenhorst, F., Lueder, T. (2000): Time and temperature variation of the intracrystalline Fe^{2+},Mg fractionation in Johnstown meteoritic orthopyroxene. *Eur. J. Mineral.*, **12**, 163–176.

Heinemann, R., Kroll, H., Kirfel, A., Barbier, B. (2003): Die Temperaturabhängigkeit der Fe^{2+},Mg-Verteilung in Olivinen. *Berichte der Deutschen Mineral. Gesellschaft, Beih. zum Eur. J. Mineral.*, **15**, 78, No 1.

Henderson, C.M.B., Knight, K.S., Redfern, S.A.T., Wood, B.J. (1996): High-temperature study of cation exchange in olivine by neutron powder diffraction. *Science*, **271**, 1713–1715.

Henderson, C.M.B., Redfern, S.A.T., Smith, R.I., Knight, K.S., Charnock, J.M. (2001): Composition and temperature dependence of cation ordering in Ni-Mg olivine solid solutions: a time-of-flight neutron powder diffraction and EXAFS study. *Am. Mineral.*, **86**, 1170–1187.

Hovestreydt, E. (1983): On the atomic scattering factor for O^{2-}. *Acta Cryst.*, **A39**, 268–269.

Kirfel, A. (1993) RINTAN. Interne R-Werte von äquivalenten und multiplen Reflexen. Universität Würzburg, Germany. Unpublished.

– (1996): Cation distributions in olivines and orthopyroxenes. An interlaboratory study. *Phys. Chem. Minerals*, **19**, 503–519.

Kroll, H. (2003) Rate equations for non-convergent order-disorder processes – a review and application to orthopyroxene. *Eur. J. Min.*, **15**, 7–19.

Kroll, H., Lueder, T., Schlenz, H., Kirfel, A., Vad, T. (1997): The Fe^{2+},Mg distribution in orthopyroxene: A critical assessment of its potential as a geospeedometer. *Eur. J. Mineral.*, **9**, 705–733.

Lager, G.A. & Meagher, E.P. (1978): High-temperature structural study of six olivines. *Am. Mineral.*, **63**, 365–377.

Le Hénaff, C., Hansen, N.K., Protas, J., Marnier, G. (1997): Electron density distribution in LiB_3O_5 at 293 K. *Acta Cryst.*, **B53**, 870–879.

Morozov, M., Brinkmann, C., Kroll, H., Lottermoser, W., Tippelt, G., Amthauer, G. (2001): Mössbauer effect study of the Mg^{2+},Fe^{2+}-distribution in synthetic olivine (fa50 fo50). *Berichte der Deutschen Mineral. Gesellschaft, Beih. zum Eur. J. Mineral.*, **13**, 127, No 1.

Morozov, M., Brinkmann, C., Lottermoser, W., Tippelt, G., Amthauer, G., Kroll, H. (2005): Octahedral cation partitioning in Mg,Fe^{2+}-olivine. Mössbauer spectroscopic study of synthetic $(Mg_{0.5}Fe^{2+}{}_{0.5})_2SiO_4(Fa_{50})$. *Eur. J. Mineral.*, **17**, 495–500

Mueller, R.F. (1967): Model for order-disorder kinetics in certain quasi-binary crystals of continuously variable composition. *J. Phys. Chem. Solids*, **28**, 2239–2243.

– (1969): Kinetics and thermodynamics of intracrystalline distributions. *Min. Soc. America, Special Paper*, **2**, 83–93.

North, A.C.T., Phillips, D.C., Mathews, F.S. (1968): A semi-empirical method of absorption correction. *Acta Cryst.*, **A24**, 351–359.

Ottonello, G., Princivalle, F., Della Giusta, A. (1990): Temperature, composition, and f_{O2} effects on intersite distribution of Mg and Fe^{2+} in olivines. *Phys. Chem., Minerals*, **17**, 301–312.

Princivalle, F. (1990): Influence of temperature and composition on Mg-Fe^{2+} intracrystalline distribution in olivines. *Mineral. Petrol.*, **43**, 121–129.

Redfern, S.A.T., Henderson, C.M.B., Wood, B.J., Harrison, R.J., Knight, K.S. (1996): Determination of olivine cooling rates from metal-cation ordering. *Nature*, **381**, 407–409.

Redfern, S.A.T., Henderson, C.M.B., Knight, K.S., Wood, B.J (1997): High-temperature order-disorder in $(Fe_{0.5}Mn_{0.5})_2SiO_4$ and $(Mg_{0.5}Mn_{0.5})_2SiO_4$ olivines: An *in situ* neutron diffraction study. *Eur. J. Mineral.*, **9**, 287–300.

Redfern, S.A.T., Artioli, G., Rinaldi, R., Henderson, C.M.B., Knight, K.S., Wood, B.J. (2000): Octahedral cation ordering in olivine at high temperature. II: An *in situ* neutron powder diffraction study on synthetic $MgFeSiO_4$ (Fa50). *Phys. Chem. Minerals*, **27**, 630–637.

Rinaldi, R. Artioli, G., Wilson, C.C., McIntyre, G. (2000): Octahedral cation ordering in olivine at high temperature. I: *In situ* neu-

tron single-crystal diffraction studies on natural mantle olivines (Fa12 and Fa10). *Phys. Chem. Minerals*, **27**, 623–629.

Robinson, K., Gibbs, G.V., Ribbe, P.H. (1971) Quadratic elongation: A quantitative measure of distortion in coordination polyhedra. *Science*, **172**, 567–570.

Scheufler, C., Engel, K.V., Kirfel, A. (1997): An improved gas-stream heating device for a single-crystal diffractometer. *Journ. Appl. Cryst.*, **30**, 411–412.

Smyth, J.R. (1975): High temperature crystal chemistry of fayalite. *Am. Mineral.*, **60**, 1092–1097.

Smyth, J.R. & Hazen, R.M. (1973): The crystal structures of forsterite and hortonolite at several temperatures up to 900 °C. *Am. Mineral.*, **58**, 588–593.

Sutanto, R.P. (2004): Untersuchungen zur Temperaturabhängigkeit der Kationenverteilung in CoMg[SiO_4]. Diploma Thesis, Mineralogisches Institut der Universität Bonn, 87 pp

Sutanto, P., Kockelmann, W., Kirfel, A. (2004): Time resolved equilibration of the cation distribution in olivine type $(Co_{0.51}Mg_{0.49})_2SiO_4$. Zeitschrift für Kristallographie, Supplement Issue No. **21**, 82

Thompson, J.B. Jr. (1969): Chemical reactions in crystals. *Am. Mineral.*, **54**, 341–375.

– (1970): Chemical reactions in crystals: Corrections and clarification. *Am. Mineral.*, **55**, 528–532.

Received 26 March 2005
Modified version received 1 December 2005
Accepted 15 September 2006